

António Nunes Vicente

# Validation of wind turbine wake models

Dissertação de Mestrado em Engenharia Mecânica  
na Especialidade de Energia e Ambiente

July/2018



UNIVERSIDADE DE COIMBRA





FCTUC FACULDADE DE CIÊNCIAS  
E TECNOLOGIA  
UNIVERSIDADE DE COIMBRA

DEPARTAMENTO DE  
ENGENHARIA MECÂNICA

## **Validation of wind turbine wake models**

Submitted in Partial Fulfilment of the Requirements for the Degree of Master in  
Mechanical Engineering in the speciality of Energy and Environment

## **Validação de modelos de esteira para turbinas eólicas**

Author

**António Henrique Seabra Nunes Vicente**

Advisors

**PhD. António Manuel Gameiro Lopes**

**PhD. Omar Herrera Sanchez (menzio GmbH)**

Jury

**President** PhD. Pedro de Figueiredo Vieira Carvalheira  
Assistant Professor, University of Coimbra

**Vowel** PhD. Almerindo Domingues Ferreira  
Assistant Professor, University of Coimbra

**Advisor** PhD. António Manuel Gameiro Lopes  
Assistant Professor, University of Coimbra



Universidade de  
Coimbra



menzio GmbH

Coimbra, July, 2018







## **ACKNOWLEDGEMENTS**

First of all, I would like to thank my advisor, Professor António Gameiro, for having given me the opportunity to work on an interesting and relevant topic. His dedication and guidance were crucial to my thesis work. I much appreciate the fact that I have always been able to made progress in a simple and steady way.

I would also like to thank my co-advisor, Professor Omar Herrera Sanchez, for his useful advice and continued support.

My time at University of Coimbra has just come to an end, and thus I would like to express my gratitude to my dearest classmates who have made my journey a pleasant one.

Last, but not the least, I would like to thank my Parents for always believing in me and pushing me to do my best, and my siblings Laura and Vasco for never letting there be a dull moment.



## **Abstract**

Wind turbine wakes have a strong impact on wind farms given that they affect the power output and the level of turbulence that determines the turbines lifetime. Thus, wake modelling is of critical importance to the wind energy industry, having a central role in the optimization of wind farm layouts.

The main objective of this work is the validation of the analytical wake models implemented in the software package WindStation. Such validation was based on measurement data recorded in an onshore wind farm with eight wind turbines, and supported by results obtained by the software package WindSim. Conclusions were drawn by analyzing the computed velocity deficit of the air flow downstream of the wind turbines and the effective power of a single wind turbine.

**Keywords:** Wind, Turbine, Wake, Turbulence, WindStation, WindSim.



## Resumo

O fenómeno de esteira tem um impacto significativo nos parques eólicos, dado que tanto a potência gerada pelas turbinas como o seu tempo de vida são afetados. Deste modo, os estudos de modelação da esteira tem uma elevada importância no seio da indústria da energia do vento, nomeadamente na otimização do layout de parques eólicos.

O principal objetivo deste trabalho é a validação de modelos de esteira analíticos implementados no software WindStation. Esta validação foi baseada em dados experimentais medidos num parque eólico terrestre com oito turbinas eólicas, e reforçada com resultados obtidos no software WindSim. As conclusões tiradas basearam-se nos resultados obtidos para o défice de velocidade do vento a montante das turbinas.

**Palavras-chave:** Vento, Turbina, Esteira, Turbulência, WindStation, WindSim.



---

## Contents

LIST OF FIGURES .....	viii
LIST OF TABLES.....	x
SIMBOLOGY AND ACRONYMS .....	11
Simbology.....	11
Acronyms.....	11
1. Introduction .....	13
2. Wind turbine wakes .....	15
2.1. Wake behavior .....	15
2.2. Wake modelling.....	16
3. Software packages .....	19
3.1. WindStation .....	19
3.1.1. Theoretical background .....	19
3.1.2. Wake models .....	22
3.1.3. Wake overlap.....	25
3.2. WindSim .....	25
4. Wind farm and measurement data .....	27
4.1. Wind farm .....	27
4.2. Measurement data .....	28
4.2.1. Filtering measurement data .....	29
5. Simulation overview .....	31
5.1. Input data .....	31
5.2. Parametrization .....	31
5.3. Important issue concerning measurement data .....	34
5.4. Panorama simulation.....	35
5.4.1. Single wake and multiple wake results.....	37
5.4.2. Offset in wind direction.....	48
5.4.3. Effective power of a wind turbine .....	50
6. Concluding remarks.....	53
References .....	55
APPENDIX A.....	57
APPENDIX B.....	59

## LIST OF FIGURES

Figure 1.1 – Global cumulative installed wind capacity (GWEC, 2017). .....	13
Figure 4.1 – Wind farm layout. ....	27
Figure 4.2 – Power curve of turbine T22. ....	30
Figure 4.3 – Rotor rpm average for turbine T22. ....	30
Figure 5.1 – Top view and lateral view of the calculation domain. ....	32
Figure 5.2 – Mesh grid analysis. ....	33
Figure 5.3 – Calculation domain parameters in WindStation (left) and WindSim (right). ..	34
Figure 5.4 – Offset in wind direction. ....	35
Figure 5.5 – WMM wind rose at 101 m (WindSim). ....	35
Figure 5.6 - Wind speed contour map obtained with Jensen model in WindStation (z=94 m; θWMM = 251°; VWMM, 101m = 7.82 m/s) .....	36
Figure 5.7 - Wind speed contour map obtained with Jensen 2D model in WindStation (z=94 m; θWMM = 251°; VWMM, 101m = 7.82 m/s).....	37
Figure 5.8 - Wind speed contour map obtained with Larsen model in WindStation (z=94 m; θWMM = 251°; VWMM, 101m = 7.82 m/s).....	37
Figure 5.9 – Jensen (WindStation) and Jensen (WindSim) panorama results for turbine T20 and wspd bin of 4-6 m/s. ....	39
Figure 5.10 - Jensen (WindStation) and Jensen (WindSim) panorama results for turbine T20 and wspd bin of 6-8 m/s.....	39
Figure 5.11 – Jensen 2D (WindStation) panorama results for turbine T20 and wspd bin of 6-8 m/s.....	40
Figure 5.12 - Jensen 2D (WindStation) panorama results for turbine T20 and wspd bin of 6-8 m/s.....	41
Figure 5.13 - Larsen (WindStation) and Larsen (WindSim) panorama results for turbine T20 and wspd bin of 4-6 m/s.....	42
Figure 5.14 - Larsen (WindStation) and Larsen (WindSim) panorama results for turbine T20 and wspd bin of 6-8 m/s.....	43
Figure 5.15 – Panorama results obtained in all wake models for turbine T20 and wspd bin of 4-6 m/s. ....	44
Figure 5.16 - Panorama results obtained in all wake models for turbine T20 and wspd bin of 6-8 m/s. ....	44
Figure 5.17 - Panorama results obtained in all wake models for turbine T9 and wspd bin of 4-6 m/s.....	46

---

Figure 5.18 - Panorama results obtained in all wake models for turbine T9 and wspd bin of 6-8 m/s.....	47
Figure 5.19 - Panorama results obtained in all wake models for turbine T6 and wspd bin of 4-6 m/s.....	47
Figure 5.20 - Panorama results obtained in all wake models for turbine T6 and wspd bin of 6-8 m/s.....	48
Figure 5.21 - Panorama results obtained in all wake models for turbine T0 and wspd bin of 4-6 m/s.....	49
Figure 5.22 – Offset correction: updated panorama results obtained in all wake models for turbine T0 and wspd bin of 4-6 m/s. ....	49
Figure 6.1 – Normalized effective wind power computed in all wake models $\theta_{WMM} = 251^\circ$ ; $V_{WMM, 101m} = 7.82$ m/s. ....	51
Figure 0.1 – WindSim 3D layout of the wind farm.....	57
Figure 0.1 - Panorama results obtained in all wake models for turbine T0 and wspd bin of 4-6 m/s.....	59
Figure 0.2 - Panorama results obtained in all wake models for turbine T0 and wspd bin of 6-8 m/s.....	60
Figure 0.3 - Panorama results obtained in all wake models for turbine T8 and wspd bin of 4-6 m/s.....	60
Figure 0.4 - Panorama results obtained in all wake models for turbine T8 and wspd bin of 6-8 m/s.....	61
Figure 0.5 - Panorama results obtained in all wake models for turbine T23 and wspd bin of 4-6 m/s.....	61
Figure 0.6 - Panorama results obtained in all wake models for turbine T23 and wspd bin of 6-8 m/s.....	62

**LIST OF TABLES**

Table 4.1 – Wind turbine technical specifications ..... 28

Table 5.1 - TI correction..... 42

Table 5.2 – Error obtained for all five wake models..... 45

Table 5.3 – Offset correction: updated error obtained for all five wake models ..... 50

Table 0.1 – Wind turbines details: row number, turbine name, turbine type, altitude (z) in meters and coordinates..... 57

## **SIMBOLOGY AND ACRONYMS**

### **Simbology**

$A$  – Wind turbine rotor swept area

$C_t$  – Thrust coefficient

$D$  – Wind turbine rotor diameter

$k$  – Turbulence kinetic energy

$r_w$  – Wake radius

$T_I$  – Turbulence intensity

$V$  – Wind speed

$V_c$  – Wind speed corrected with the wake effect

$V_{def}$  – Wind speed deficit

$V_\infty$  – Free stream wind speed

$WDC$  – Wake decay constant

$\theta$  – Wind direction

### **Acronyms**

GWEC – Global Wind Energy Council

SCADA – Supervisory Control And Data Acquisition

WFDT – Wind Farm Design Tool

WMM – Wind Meteorological Mast

wspd – Wind speed



## 1. INTRODUCTION

Although fossil fuels are still the dominant source of energy, there has been a gradual shift towards renewable energies. One of the most reliable sustainable energy is wind energy, which nowadays is used in large scale for electrical power production. The global cumulative installed wind power capacity in 2017 has overcome the value of 500,000 MW (see Figure 1.1). This power is produced in onshore and offshore wind farms containing large numbers of wind turbines.

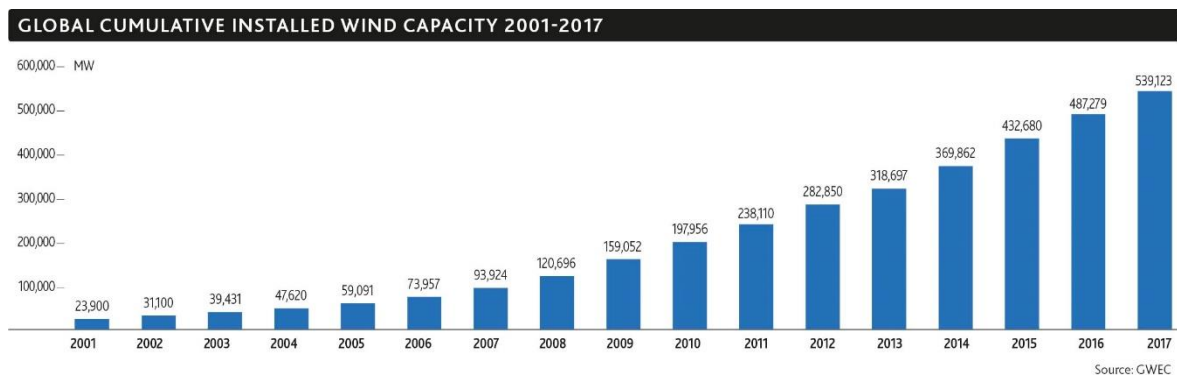


**Figure 1.1 – Global cumulative installed wind capacity. Adapted from GWEC (2018)**

The concept of energy conservation dictates that if a wind turbine extracts kinetic energy from the wind, then the downstream flow will diminish in momentum. The turbine wake is the region affected by this momentum deficit. Due to wake effects, wind turbines positioned downstream of others will have its performance considerably affected: lower wind speeds reduce the turbine power generation, and the raise of turbulence intensity causes fatigue loads, shortening the turbine life span. Owing to the cost of land, wind turbines are being grouped together in tighter spacing, which leads to increased wake effects. Hence, wake modelling plays a central role in developing optimized wind farm layouts.

The goal of this work is to validate and evaluate the wake models included in the software package WindStation. Measurement data from a small onshore wind farm will be used to assess the prediction of the velocity deficit for each wake model. The validation of these models is then corroborated by the software package WindSim.

The outline of this thesis is as follows. Chapter 2 will give an introduction to turbine wakes and its modelling background. Chapter 3 will provide a description of

WindStation and its available wake models, as well as a short overview of WindSim. The measurement data of the wind farm will be presented in Chapter 4, together with the filtering process made with such data. Chapter 5 then discusses the validation of the wake models: the focus is on comparing the velocity deficit results obtained by a panorama calculation in WindStation and WindSim with measurement data. Both single wake and multiple wake situations are analysed. The effective power of single turbines will also be analysed.

## 2. WIND TURBINE WAKES

This chapter will provide a brief description of the wake behavior, from its beginning to a further downstream position, as well as a summary of the wake modelling background.

### 2.1. Wake behavior

As the air flow approaches a wind turbine, it starts to slow down and the pressure increases. Then, when it crosses the turbine rotor, there is a sudden pressure drop (see Figure 2.1, cut A-A).

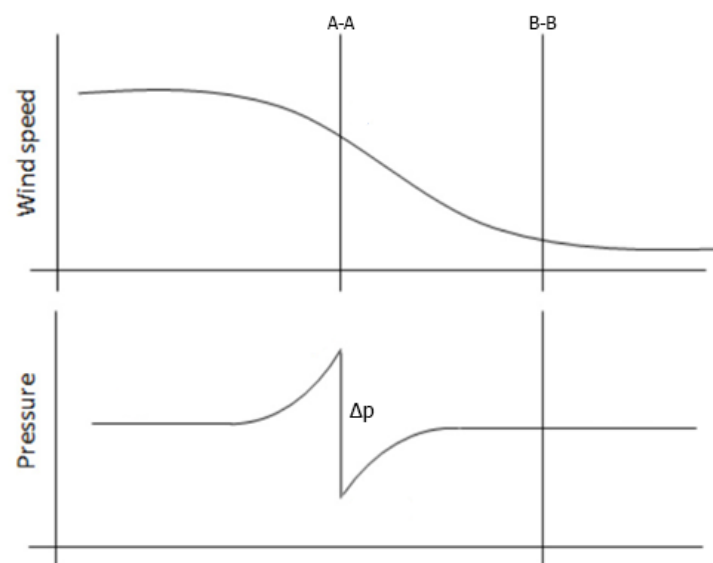


Figure 2.1 – Wind speed and pressure variation. Adapted from Janssen (2012).

A turbine wake region is commonly divided into a near wake and a far wake. The region immediately downstream of the rotor is called the near wake and it extends for 2 to 5 rotor diameters. This region is dominated by the turbulence created by the turbine itself: there are non-uniform deficits of pressure and wind speed associated with the axial thrust and torque of the machine. The air circulation along the turbine blades leads to the formation of vortices with helical trajectories that quickly expand, forming a cylindrical shear layer. This shear layer is what separates the inside of the wake from the outside

ambient flow. Figure 2.2 depicts a sketch of this situation. The wake growth and shear layer expansion are represented based on an axisymmetric flow.

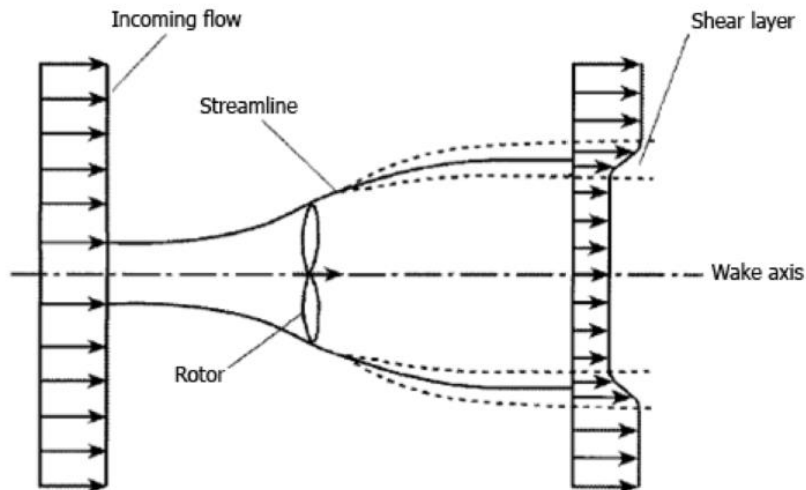


Figure 2.2 – Wake growth based on an axisymmetric flow. Adapted from Crespo et al. (1999).

Further downstream, the wake starts to recover: the pressure increases and the velocity inside the wake decreases until ambient pressure is reached (Figure 2.1, cut B-B). As turbulent diffusion of momentum becomes the dominant mechanism, the near wake region ends when the shear layer thickness increases until it reaches the wake axis.

The far wake region starts approximately 5 diameters behind the rotor, where the wake flow is completely developed. The wind velocity starts then to recover and the flow will decay to its free stream conditions. The topographic effects and ambient turbulence become dominant over the turbulence caused by the rotor.

## 2.2. Wake modelling

A significant amount of research has been done over the past 50 years in wake modelling. A comprehensive literature survey on wake models can be found in Crespo et al. (1999). They distinguished two classic approaches to the problem. A common approach was to assume that the turbines acted as distributed roughness elements. These models used a logarithmic wind profile, modified by an increase in roughness due to the presence of the turbine itself; see, e.g., Bossanyi et al. (1980), Emeis and Frandsen (1993).

However, the traditional approach to wake modelling is based on the description of a single wake, succeeded by a calculation of its interaction with the neighbouring ones. These type of models are known as individual models. The classical work by Lissaman (1979) was one of the pioneers of this method. The author described a computer model for an arbitrary array of turbines, using basic fluid mechanics expressions and self-similar wake profiles derived from the experimental work done by Abramovich (1963) on co-flowing jets.

Individual wake models are divided into two categories: analytical models and computational models. Other authors call them kinematic models and field models, respectively.

Computational models are very time consuming and computationally expensive, as they make the least simplifications of the Navier-Stokes equations to fully characterize the turbine wake and turbulence. These models calculate the flow magnitudes at every point of the flow field, with resource to Computational Fluid Dynamics (CFD). Relevant field models were developed by Taylor (1980), Ainslie (1985), and Crespo and Hernández (1989). According to Réthoré (2009) there are three main CFD wind turbine wake models: full-rotor computations, the actuator line method and the actuator disk method. However, these type of models will not be studied in this work.

Analytical wake models are based on semi-empirical functions and simplifications of the Navier-Stokes equations. They apply analytical expressions to calculate the wind speed deficits after the calculation of wind fields. Different models have been presented in the past years; see, e.g., Lissaman (1979), Jensen (1983), Frandsen (2007) and Ishihara et al. (2004). These models can be very effective in modelling the wake expansion and the velocity deficit, and are usually preferred due to its computational efficiency and fastest resolution. However, as the change in ambient turbulence is not considered, a turbulence model has to be coupled with analytical models.

WindStation provides three (analytical) wake models: Jensen, Jensen 2D and Larsen. These models will be introduced in the following chapter.



### 3. SOFTWARE PACKAGES

In this chapter the software packages that were used on this work are described: WindStation and WindSim. The main focus is on describing WindStation, with reference to the main theoretical foundation concepts and available wake models.

#### 3.1. WindStation

WindStation is a software package for the numerical simulation of turbulent flow over complex topography, complemented with a recent update of turbine wake modelling. The numerical wind fields are calculated with provided solutions for the non-linear fluid dynamics equations, coupled with turbulence models. Detailed information about WindStation is available in the WindStation manual by Lopes (2018).

##### 3.1.1. Theoretical background

###### 3.1.1.1. Transport equations

The numerical calculation is supported by the non-linear fluid dynamics equations, more specifically the Navier-Stokes equations, the continuity equation and the energy equation. A summary of these equations will be made next.

The Navier-Stokes equation describes the conservation of momentum for a fluid flow, with the assumption that it is a function of a pressure term and a diffusion viscous term. The generic WindStation steady state formulation of these equations is:

$$\frac{\partial}{\partial x_j} (\rho u_i u_j) = -\frac{\partial p}{\partial x_i} + \frac{\partial}{\partial x_j} \left[ \Gamma \left( 2 \frac{\partial u_j}{\partial x_j} - \frac{2}{3} \text{div} \vec{V} \right) \right] + \frac{\partial}{\partial x_j} \left[ \Gamma \left( 2 \frac{\partial u_i}{\partial x_j} + \frac{\partial u_j}{\partial x_i} \right) \right] + \left( \rho g \beta (T - T_{ref}) \right)_{i=3} + S_{ci} + S_{ui} \quad (3.1)$$

where  $\rho$  [kg/m<sup>3</sup>] is the fluid density,  $x_i$  [m] is a generic Cartesian coordinate,  $p$  [N/m<sup>2</sup>] is the pressure, and  $\Gamma = \mu_{eff} = \mu + \mu_t$  [N s/m<sup>2</sup>] is the time diffusion coefficient for momentum, i.e., the effective viscosity.

Coriolis effects (caused by the earth's rotation) are included by adding an additional term to the  $u$  ( $i=1$ ; west-east direction) and  $v$  ( $i=2$ ; south-north direction) equations. These are:

$$\begin{aligned} S_{c1} &= -f_c \rho v \\ S_{c2} &= f_c \rho u \\ S_{c3} &= 0 \end{aligned} \quad (3.2)$$

and where  $f_c$  is the Coriolis term, given by

$$f_c = 2\Omega \sin\lambda \quad (3.3)$$

with  $\Omega$  as the earth's rotation rate and  $\lambda$  representing the local latitude.

The source term  $S_{ui}$  accounts for the presence of porous obstacles such as trees or bushes, and is computed with a forest model. Buoyancy forces are included, where  $T$  [K] is the potential temperature (corresponding to the adiabatic vertical temperature gradient),  $T_{ref}$  is a reference potential temperature and  $\beta = T_{loc}^{-1}$  is the thermal expansion coefficient, with  $T_{loc}$  as the local temperature.

The continuity equation represents the mass conservation:

$$\frac{\partial(\rho u_j)}{\partial x_i} = 0 \quad (3.4)$$

The energy equation is written for potential temperature as the dependent variable:

$$\frac{\partial}{\partial x}(\rho c_p u T) + \frac{\partial}{\partial x}(\rho c_p w T) = \frac{\partial}{\partial x}\left(\Gamma \frac{\partial T}{\partial x}\right) + \frac{\partial}{\partial z}\left(\Gamma \frac{\partial T}{\partial z}\right) \quad (3.5)$$

The diffusion coefficient is (for the case of a fluid domain):

$$\Gamma = \left(\frac{\mu}{Pr} + \frac{\mu}{\sigma_T}\right) c_p \quad (3.6)$$

where  $Pr = 0.71$  and  $\sigma_T$  are the laminar and the turbulent Prandtl numbers, respectively. The turbulent Prandtl number value depends on the adopted turbulence model.

### 3.1.1.2. Turbulence models

WindStation has four implemented turbulence models, all four being different versions of the  $k - \epsilon$  turbulence model. These turbulence models compute the turbulent viscosity making use of the transport equations. The models are the following:

- Standard  $k - \epsilon$  model
- RNG  $k - \epsilon$  model
- Realizable  $k - \epsilon$  model
- Limited-length  $k - \epsilon$  model

The standard model defines the turbulent viscosity by:

$$\mu_t = C_\mu \frac{\rho k^2}{\epsilon} \quad (3.7)$$

where  $k$  [ $\text{m}^2/\text{s}^2$ ] is the turbulence kinetic energy, which is a measure of the flow turbulence intensity  $T_I$ :

$$T_I = \frac{\sqrt{\frac{2}{3}k}}{V} \Rightarrow k = \frac{3}{2}(T_I V)^2 \quad (3.8)$$

where  $V$  [ $\text{m}/\text{s}$ ] is the velocity magnitude. The dissipation rate of turbulence kinetic energy,  $\epsilon$  [ $\text{m}^2/\text{s}^3$ ] is related to the dissipation length scale  $L_d$  as follows:

$$L_d = C_\mu^{3/4} \frac{k^{3/2}}{\epsilon} \Rightarrow \epsilon = C_\mu^{3/4} \frac{k^{3/2}}{L_d} \quad (3.9)$$

The turbulence kinetic energy and its dissipation rate are computed by the transport equations, with different considerations depending on the model. During this work, the Limited-length  $k - \epsilon$  model was the chosen one, due to its inclusion of Coriolis terms. More details about WindStation turbulence models can be consulted at the user's manual by Lopes (2018).

### 3.1.1.3. Numerical solution

The flow solution takes place in a structured mesh with uniform spacing in the horizontal ( $x, y$ ) direction, and a variable vertical spacing defined by an expansion factor. The transport equations are transformed from their original Cartesian form into a generalized coordinate form using the chain rule (see Patankar, 1980).

The equations are then discretized and integrated using a control volume approach. For the advection terms, two advection schemes are implemented in Wind Station, being the hybrid scheme by Patankar (1980) and the third-order scheme QUICK by Hayase (1992). After integration, the equations are cast in the following general algebraic form:

$$a_p \phi_p = \sum_{nb} a_{nb} \phi_{nb} + b \quad (3.10)$$

This equation relates the value of the generic variable  $\phi$  (velocity components, turbulence quantities or temperature) at location  $P$  to its neighbor ( $nb$ ) values. The  $b$  term is a source term.

The equations are then solved numerically using the SIMPLEC algorithm by Van Doormaal and Raithby (1984), which is a modification of the original SIMPLE algorithm proposed by Patankar (1980).

### **3.1.2. Wake models**

#### **3.1.2.1. Jensen wake model**

The Jensen wake model was first developed by N.O. Jensen (1983). According to this model, the wake behind a wind turbine expands linearly, and the velocity deficit is only dependent on the distance downstream from the turbine. Its uniform velocity profile shape is often called top-hat. A simpler version of this model was presented later by Katic et al. (1987).

The wake radius is given by:

$$r_w = \frac{D}{2} (1 + 2WDCs) \quad (3.11)$$

where

- $D$  is the rotor diameter of the wind turbine;
- $s = x/D$  is the relative distance behind the rotor;
- $x$  is the downstream distance from the turbine;
- $WDC$  is the wake decay constant.

The velocity deficit  $V_{def}$  is computed at each point in the field by the following equation:

$$V_{def} = \frac{1 - \sqrt{1 - C_t}}{(1 + 2WDCs)^2} \quad (3.12)$$

where  $C_t$  is the wind turbine thrust coefficient, computed from the turbine characteristic curve. The wind speed corrected for wake effects is:

$$V_c = V(1 - V_{def}) \quad (3.13)$$

Note that the Jensen model is not designed for near wake, as it assumes a fully turbulent flow. It should be applied at a minimum distance of 3 rotor diameters.

### 3.1.2.2. Jensen 2D wake model

Tian et al. (2015) proposed a correction for the Jensen model, the Jensen 2D model. It is based on a sinusoidal correction as function of the distance  $r$  to the wake center line. Similarly to the Jensen model, the wake expands linearly. However, the velocity profile in the wake cross section has a cosine shape distribution instead of a top hat shape.

The corrected wind speed deficit is given by:

$$(V_{def})_{2D} = V_{def} \left[ 1 - \cos \left( \frac{\pi \times r}{r_w} + \pi \right) \right] \quad (3.14)$$

where  $r$  is the radial distance from the center of the wake and  $V_{def}$  is the velocity deficit predicted in the original Jensen wake model.

### 3.1.2.3. Wake decay constant for Jensen and Jensen 2D wake models

The critical problem about using the Jensen and Jensen 2D wake models, is how to determine the WDC. For the Jensen model, several authors proposed different values for the WDC, the most common ones being 0.075 for onshore wind farms and 0.05 for offshore wind farms. In this work, the Jensen model will always be computed with  $WDC = 0.075$  (both in WindStation and in WindSim).

For the Jensen 2D wake model, WindStation allows the user to choose between a specific value of WDC or to compute it from two other ways: the *hub TI* or the *hub  $z_0$* :

- *hub  $z_0$*  – Tian et al. (Tian et al. 2015) proposed the following empirical expression for WDC:

$$WDC = 0.5/\ln\left(\frac{z}{z_0}\right) \quad (3.15)$$

where  $z$  is the hub height of the wind turbine and  $z_0$  is the surface roughness height of a local terrain. However, the author himself said that this equation may not be reliable because only the ambient turbulence is considered, hence missing the turbine-induced turbulence.

- *hub*  $T_I$  – Another possibility is to obtain the WDC from the turbulence intensity at the hub location,  $T_{I,hub}$ :

$$WDC = 0.5T_{I,hub} \quad (3.16)$$

#### 3.1.2.4. Larsen wake model

The Larsen wake model was proposed by Larsen (1988). The model is based on the Prandtl turbulent boundary layer equations and has variable expansion rate for the wake that accounts for the ambient turbulence.

The wake radius is given by:

$$r_w = 2 \left(\frac{35}{2\pi}\right)^{1/5} (3c_1^2)^{1/5} [C_t A(x + x_0)]^{1/3} \quad (3.17)$$

The wind speed deficit is given by:

$$V_{def} = \frac{V_\infty}{9} [C_t A(x + x_0)^{-2}]^{1/3} \left\{ r^{3/2} [3c_1^2 C_t A(x + x_0)]^{-1/2} - \left(\frac{35}{2\pi}\right)^{3/10} (3c_1^2)^{-1/5} \right\}^2 \quad (3.18)$$

Where  $V_\infty$  is the free stream wind speed;  $c_1$ ,  $x_0$ ,  $D_{eff}$ ,  $R_{9.5}$  and  $R_{nb}$  are given by:

$$c_1 = \left(\frac{D_{eff}}{2}\right)^{5/2} \left(\frac{105}{2\pi}\right)^{-1/2} (C_t A x_0) \quad (3.19)$$

$$x_0 = \frac{9.5D}{\left(\frac{2R_{9.5}}{D_{eff}}\right)^3 - 1} \quad (3.20)$$

$$D_{eff} = D \sqrt{\frac{1 + \sqrt{1 - C_t}}{2\sqrt{1 - C_t}}} \quad (3.21)$$

$$R_{9.5} = 0.5[R_{nb} + \min(H, R_{nb})] \quad (3.22)$$

$$R_{nb} = \max(1.08D, 1.08D + 21.7D(T_{I,amb} - 0.05)) \quad (3.23)$$

In the previous equations,  $H$  is the turbine height,  $A$  is the rotor area and  $T_{I,amb}$  is the ambient turbulence intensity.

### 3.1.3. Wake overlap

When more than one turbine influences the velocity at the considered location, the velocity deficits calculated by the analytical wake models are combined to obtain an equivalent wake velocity deficit. WindStation uses the square root of the sum of the squares, given by equation 3.24. This method is equally used in WindSim:

$$V_{def} = \sqrt{\sum_{i=1}^{ntot} (V_{def,i})^2} \quad (3.24)$$

To compute the turbine power, the effective wind speed deficit must be calculated. It takes into account the overlap area between the rotor and the wake:

$$V_{def,effective} = V_{def} \frac{A_{overlap}}{A} \quad (3.25)$$

## 3.2. WindSim

WindSim is a modern Wind Farm Design Tool (WFDT). It is used to optimize the wind farm energy production while keeping the turbine loads within acceptable limits. This optimization process, called micrositeing, is achieved by calculating numerical wind fields over a digitalized terrain. This software uses a modular approach with six modules to complete the steps of a full micrositeing. The six modules are:

- Terrain – the 3D model of the terrain is generated, based on elevation and roughness data;

- Wind Fields – the numerical wind fields are calculated based on boundary conditions, turbulence models and calculation parameters;
- Objects – the wind turbines and climatology data are placed and processed;
- Results – the wind field simulation results can be stored and analyzed;
- Wind Resources – the wind field numerical results are coupled with climatology data to provide a wind resource map;
- Energy – the annual energy production, AEP, is calculated for all turbines, including wake losses.

In this work, WindSim was used as an alternative approach to WindStation for assessing the wake models. The procedure was to replicate, as far as possible, the simulation parameters used on WindStation. WindSim provides three wake models: Jensen, Larsen, and a third one with a turbulent dependent rate of wake expansion (which was not used in this work). More details about WindSim can be found in the *WindSim Getting Started* manual by Meissner (2015).

## 4. WIND FARM AND MEASUREMENT DATA

### 4.1. Wind farm

The wind farm under study in this work is located in northern France and is composed by eight wind turbines and one meteorological mast (WMM), displayed as in Figure 4.1. A 3D layout from WindSim of the wind farm is also available in Figure 0.1 of APPENDIX A. The turbines are arranged in two rows: row 1 (composed by  $T_{21}, T_{20}, T_9, T_6$ ) and row 2 (composed by  $T_{22}, T_0, T_8, T_{23}$ ). The meteorological mast is placed southwest of the array. Detailed information regarding turbine coordinates and mean sea level height is available in Table 0.1 of APPENDIX A.

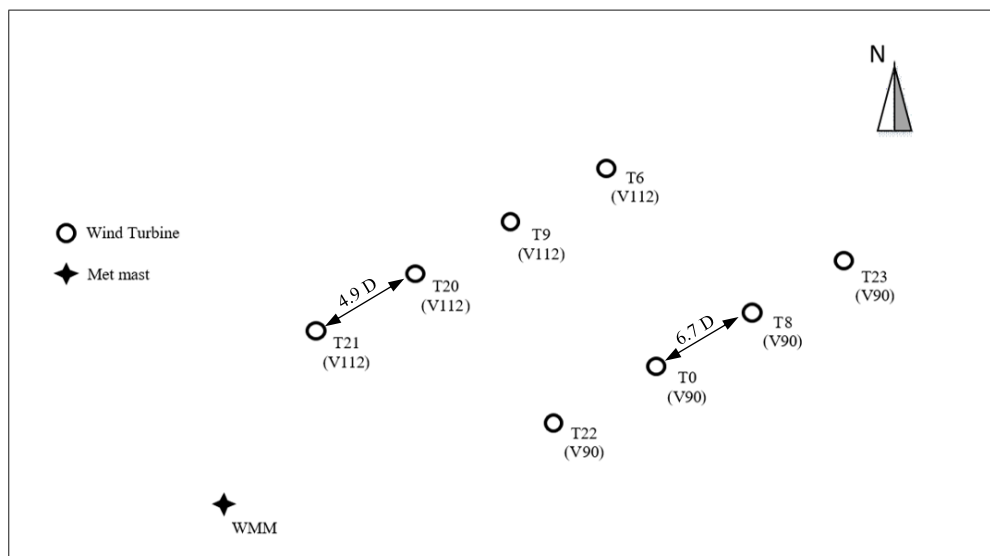


Figure 4.1 – Wind farm layout.

The turbine types are *Vestas V90* – 2.0 MW and *Vestas V112* – 3.075 MW. Row 1 is composed by the *V90* type and row 2 by *V112*. Its main technical specifications are displayed in the following table:

**Table 4.1 – Wind turbine technical specifications**

Turbine	Rated power (kW)	Cut-in wind speed (m/s)	Cut-out wind speed (m/s)	Rotor diameter (m)	Hub height (m)
V90	2000	4	25	90	105
V112	3075	3	25	112	94

The wind farm array is irregularly spaced. The spacing between turbines in a row range from a minimum distance of 548 m for  $T21 - T20$ , which corresponds to 4.9 rotor diameters ( $4.9 D$ ), to a maximum distance of 601 m ( $6.2 D$ ) for  $T0 - T8$  (see Figure 4.1). On the other hand, adjacent turbines are separated by a minimum distance of 1642 m ( $14,7 D$ ) for  $T6 - T23$  and a maximum distance of 1872 m ( $16,7 D$ ) for  $T21 - T22$ . As for the meteorological mast, its closest wind turbine is  $T21$  at 1599 m.

Note that this wind farm is neighbored by 3 other ones, which will not be considered throughout this study due to inexistent measurement data.

## 4.2. Measurement data

For this investigation, the available data was SCADA data, recorded during the month of August 2016. The dataset is composed by 10-minute mean values measured in the 8 wind turbines and in the meteorological mast.

The wind turbine measurements were made at hub height. The variables measured for each turbine were the following:

- *Wind speed* [m/s]
- *Nacelle direction* [°]
- *Ambient wind direction* [°]
- *Power production* [kW]
- *Status of wind turbine*
- *Blades pitch angle* [°]
- *Rotor rotation speed* [rpm]
- *Ambient temperature* [°C]

The meteorological mast measurements were made at 5 different heights: 40 m, 60 m, 80 m, 99 m and 101 m. The variables measured for each height were the following:

- *Mean wind speed* [m/s]
- *Wind direction* [°]

- *Wind speed standard deviation*
- *Wind direction standard deviation*

The turbulence intensity in the meteorological mast at a height of  $z$  can be defined by equation 4.1:

$$T_{I,z} = \frac{\sigma(z)}{V_{\infty}(z)} \quad (4.1)$$

where  $\sigma(z)$  is the wind speed standard deviation and  $V_{\infty}(z)$  is the free stream wind speed, both at height  $z$ . This way of computing the turbulence intensity will be discussed later.

Furthermore, two *trb* files with information about the *V90* and the *V112* wind turbines were provided. The information included the hub height, rated power, rotor diameter, and measured values for both power and thrust coefficient curves as function of wind speed.

#### **4.2.1. Filtering measurement data**

Filtering measurement data is an important part of the validation process. It is known that several external factors can influence the measurements accuracy, such as turbulence, air density, wind speed gradients, wind turbine technical problems, etc. In a report of flow and wakes in large wind farms by Barthelmie et al. (2011), a description is provided for the authors' experience in organizing and filtering data from large wind farms. A previous paper (Réthoré et al., 2009) proposed a general guideline for data validation.

This section describes all the filtering process made in this work when using SCADA data. The starting point was to eliminate all wind speed values lower than the cut-in wind speed, i.e.,  $V < 3$  m/s for *V112* turbines and  $V < 4$  m/s for *V90* turbines. The negative power production values were also all eliminated.

Nacelle misalignment is an important factor to take in consideration. It can be defined as the difference between the ambient wind direction at hub height and the nacelle direction. Time records with registered values above  $5^\circ$  were eliminated.

Furthermore, a comparison between the real power curve of each wind turbine (obtained with measurement data) and the one provided by the *trb* file was made. Taking

turbine T22 as an example, Figure 4.2 shows both power curves (real and *trb* file) in one chart. The points away from the power curve were eliminated.

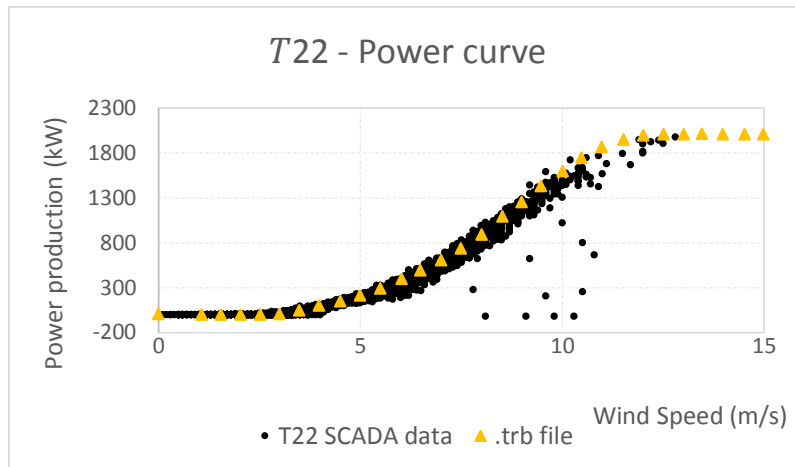


Figure 4.2 – Power curve of turbine T22.

Other parameters taken into consideration were the rotor rotation speed and the blades pitch angle. By plotting these variables with ambient wind speed, one can evaluate whether the turbine is working normally. See for instance the rotor rotation speed in Figure 4.3 - the points away from the curve were eliminated.

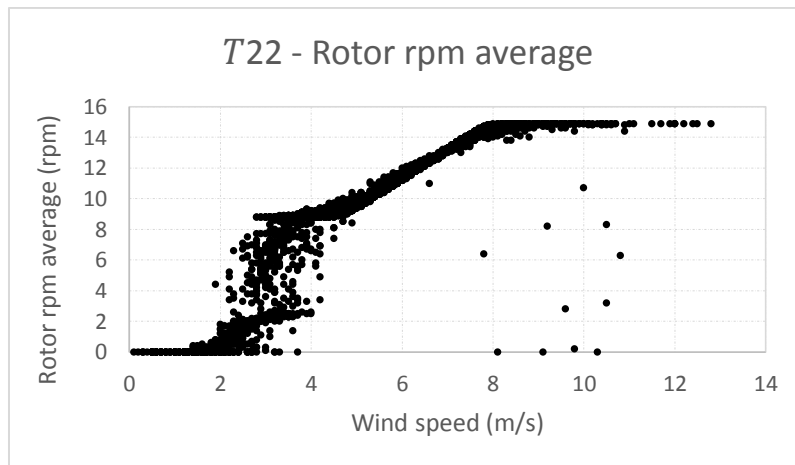


Figure 4.3 – Rotor rpm average for turbine T22.

## 5. SIMULATION OVERVIEW

### 5.1. Input data

The input data for both WindStation and WindSim consisted on the terrain data of the site, the meteorological mast data, and the wind turbine data stored in the *trb* files already mentioned in Section 4.2. The terrain data was composed by the elevation and roughness files which were converted from WindStation file format, *ArcInfo* ASCII, to WindSim format *gws*, using the *Global Mapper* software package (see Global Mapper 19.1).

In WindStation, the initialization of the wind fields is done by assigning velocity, turbulence and temperature values for the whole domain. In this case, those values are based on the meteorological mast data. Then, a reconstruction of the vertical profiles is done for both wind speed and turbulence quantities. This reconstruction may be done with two different approaches, depending whether the Coriolis forces are considered or not. In this work, Coriolis forces were always considered. The remaining calculation process depends on the boundary conditions and other parametrization. For more details please see Lopes (2018).

### 5.2. Parametrization

**Domain extension.** The calculation domain is nearly parallelepipedic. It is delimited at the bottom by the ground and at the top by a horizontal plane. The area covered by the whole terrain data is huge (roughly  $6659 \text{ km}^2$ ), which naturally led to a reduction of the calculation domain extension (into an area of  $37 \text{ km}^2$ ). Figure 5.1 shows the top view of the actual calculation domain in WindStation, and a lateral view through cut A-B.

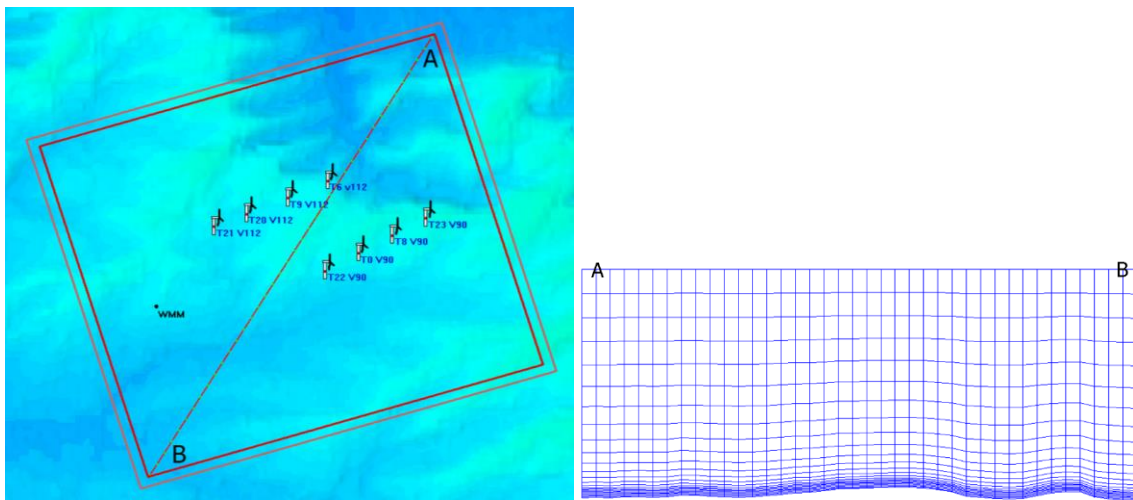


Figure 5.1 – Top view and lateral view of the calculation domain.

**Mesh.** The mesh in WindStation is defined by a constant horizontal spacing and a variable vertical spacing. In order to choose a value for the horizontal spacing, a mesh refinement analysis was performed by reducing the horizontal spacing from 1000 m to 20 m. The expectation was that a mesh refinement would not have much influence on the results, because the terrain is rather smooth and the measurements are done at a relevant distance from the ground. The chosen turbine was *T22*, with an ambient wind direction corresponding to an undisturbed incoming flow ( $\theta_{T22} = 234.2^\circ$ ). Figure 5.2 plots both the measured wind speed and the one obtained in WindStation, together with the number of nodes. As expected, the mesh influence on result accuracy is hardly perceptible (note that the vertical axis values only range between 4,9 m/s and 5,1 m/s). However, the optimal solution fell on a horizontal spacing of 40 m, with a number of nodes approximately equal to 500,000. Although a 20 m spacing could provide a vaguely better agreement with measured data, one would increase significantly the number of nodes, leading to an excessive computational time. The 40 m spacing showed a good balance between accuracy and simulation time.

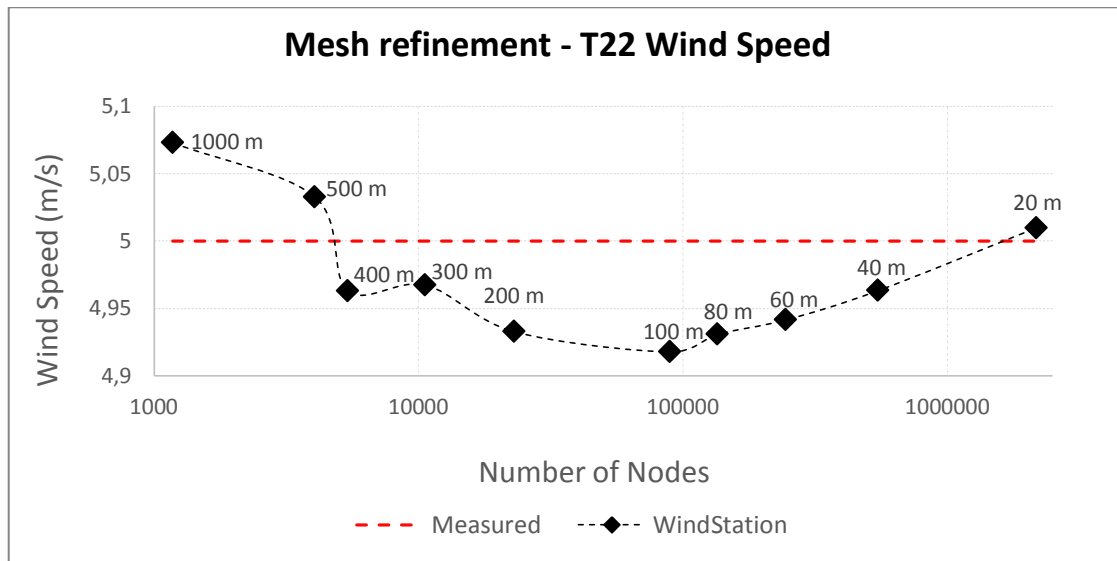


Figure 5.2 – Mesh grid analysis.

The vertical spacing in WindStation is defined by the altitude (above sea level) of the calculation domain top ( $Z_{top}$ ), by the vertical distance between the first calculation point and the ground (*First node*), and by the number of calculation levels (*Levels*). The *Max vertical spacing* is the height of last control volume. As shown in Figure 5.3, these parameters slightly differ from WindStation to WindSim. The difference between  $Z_{top}$  and *Height above terrain* is given by:

$$\text{Height above terrain} = Z_{top} - \text{Altitude} \quad (5.1)$$

The *Height distribution factor* gives the fraction between the cell at the ground and the cell at the upper boundary:

$$\text{Height distribution factor} = \frac{\text{First node}}{\text{Max vertical spacing}} \quad (5.2)$$

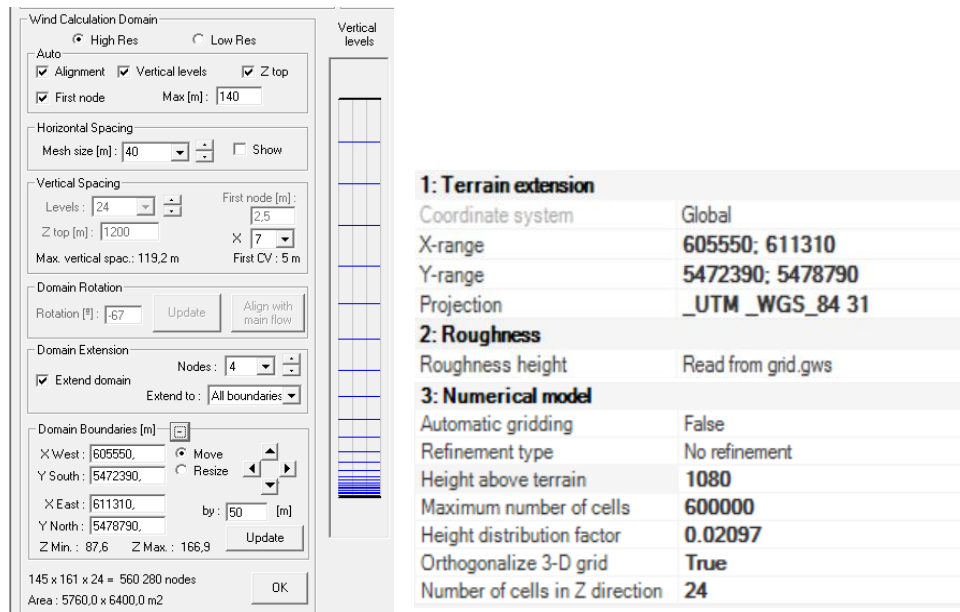


**Figure 5.3 – Calculation domain parameters in WindStation (left) and WindSim (right). Note that the altitude of the calculation domain top is equal to Ztop=1200 m.**

### 5.3. Important issue concerning measurement data

The major setback when using the meteorological WMM mast data as an input parameter was dealing with discrepancies between its values and the ones from wind turbines. In fact, if a wind direction measured in the mast is considerably different from the one measured in the wind turbines, the modelled wind flow can account for a multiple wake superposition situation, when in reality it is not. Figure 5.4 plots the *WMM wind direction* at a height of 101 m with the *ambient wind direction* [°] at turbine T0. This was done for the wind direction interval of  $\theta \in [200^\circ, 280^\circ]$ . The offset in wind direction was found to be large and for some cases reaches a value of 40°.

In this way, it was concluded that it is rather difficult to use the meteorological mast data as a reference value for the wind turbine when analysing the simulated results. Instead, the upstream wind turbine was used.

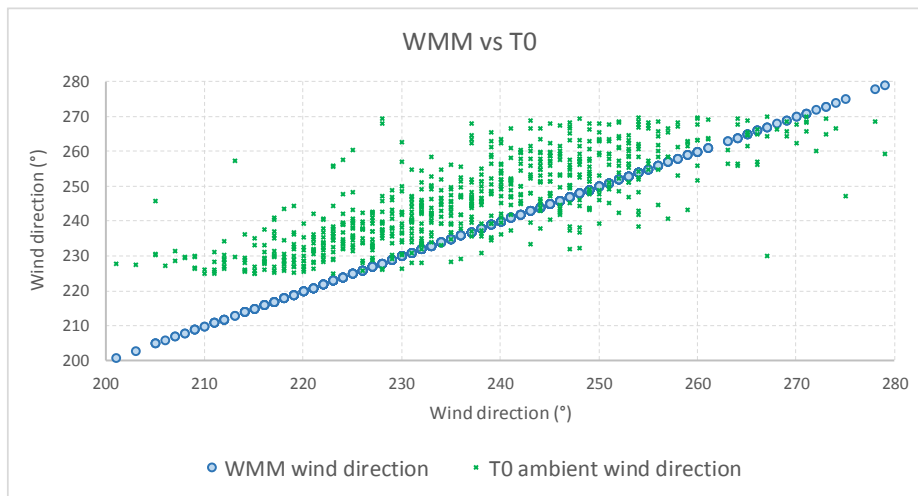


Figure 5.4 – Offset in wind direction.

## 5.4. Panorama simulation

Figure 5.5 is a wind rose taken from the climatology report of WindSim. It gives the wind speed distribution in the WMM at a height of 101 m, divided in bins of 2 m/s and wind direction sectors of 30°. It is clear that the most common wind direction sectors correspond to an air flow from southwest.

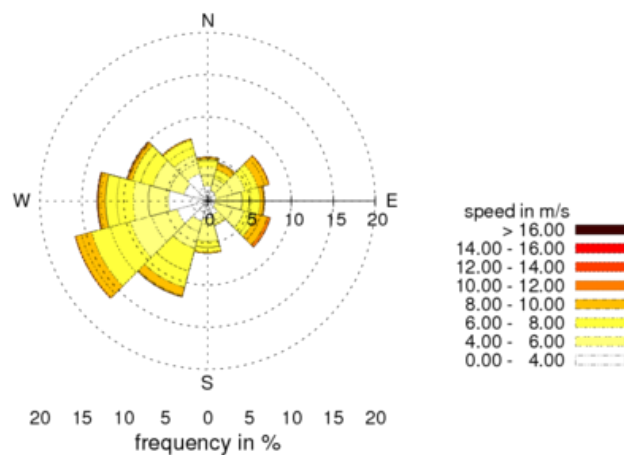


Figure 5.5 – WMM wind rose at 101 m (WindSim).

Based on the sector availability of the WMM measured data (displayed in the wind rose) a panorama simulation was performed for a wind direction interval of  $\theta \in [225^\circ; 270^\circ]$  and the results were separated in two wind speed bins: 4 – 6 m/s and 6 – 8 m/s. Wind speeds above 8 m/s were not considered due to lack of measurement data. The goal of this simulation was to investigate the velocity deficit at hub height for each turbine.

The distinction between a single wake and a multiple wake situation will be presented in the following section.

Figure 5.6 represents a multiple wake superposition situation ( $\theta_{WMM} = 251^\circ$ ;  $V_{WMM,101m} = 7.82 \text{ m/s}$ ). It is a contour map of wind speed computed with the Jensen model at the V112 hub height (94 m), obtained with WindStation. Note that turbine T21 is not affected by other turbine wakes, while turbines T20, T9 and T6 are respectively in a simple, double and triple wake superposition region. When comparing it with Figure 5.7 and Figure 5.8, obtained respectively with Jensen 2D and Larsen model, it is clear that the wake region downstream of turbine T6 (quadrupole wake region) seems to spread farther in the Larsen model.

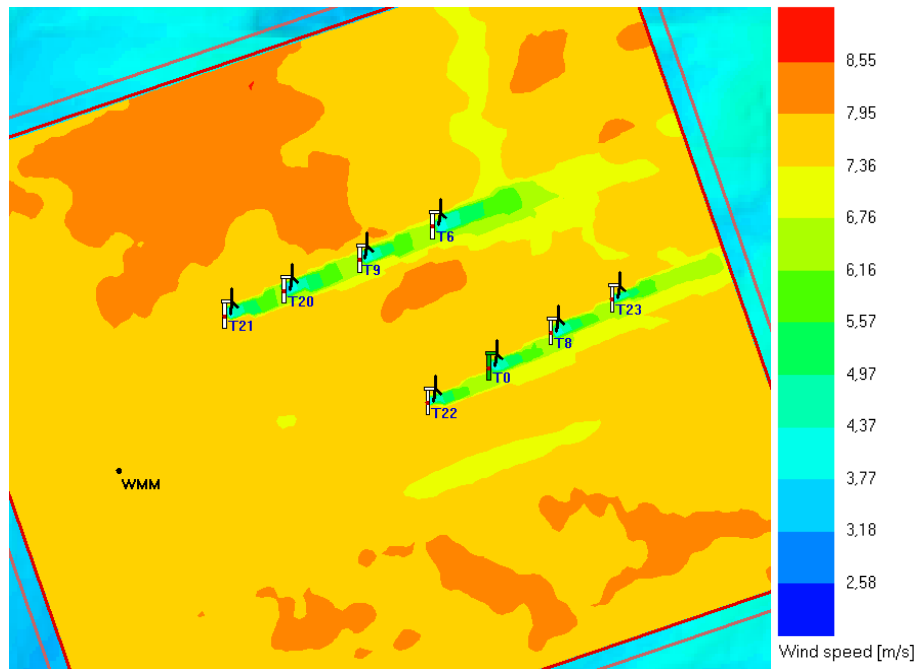


Figure 5.6 - Wind speed contour map obtained with Jensen model in WindStation ( $z=94 \text{ m}$ ;  $\theta_{WMM} = 251^\circ$ ;  $V_{WMM,101m} = 7.82 \text{ m/s}$ )

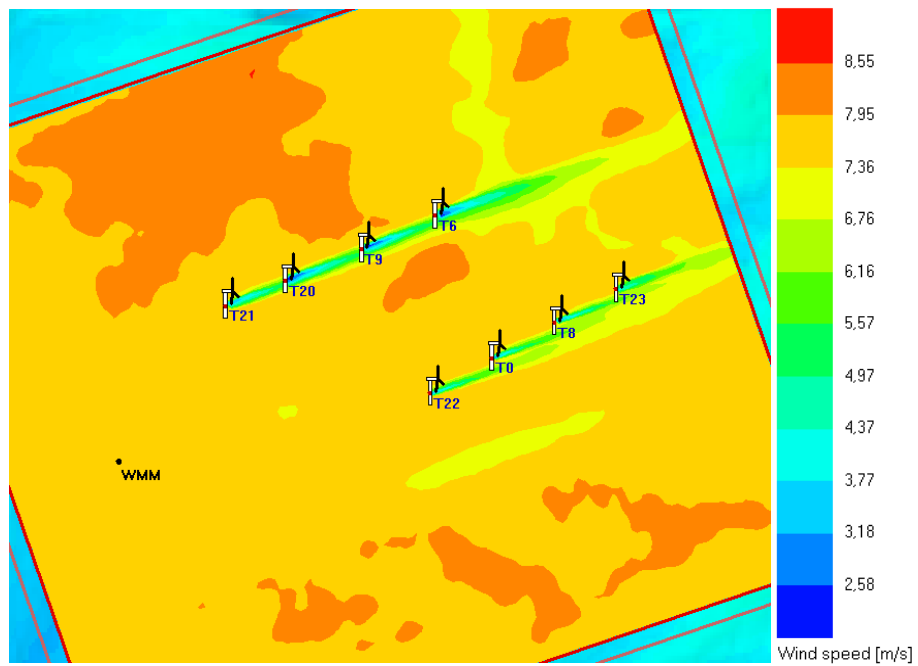


Figure 5.7 - Wind speed contour map obtained with Jensen 2D model in WindStation ( $z=94$  m;  $\theta_{WMM} = 251^\circ$ ;  $V_{WMM,101m} = 7.82$  m/s)

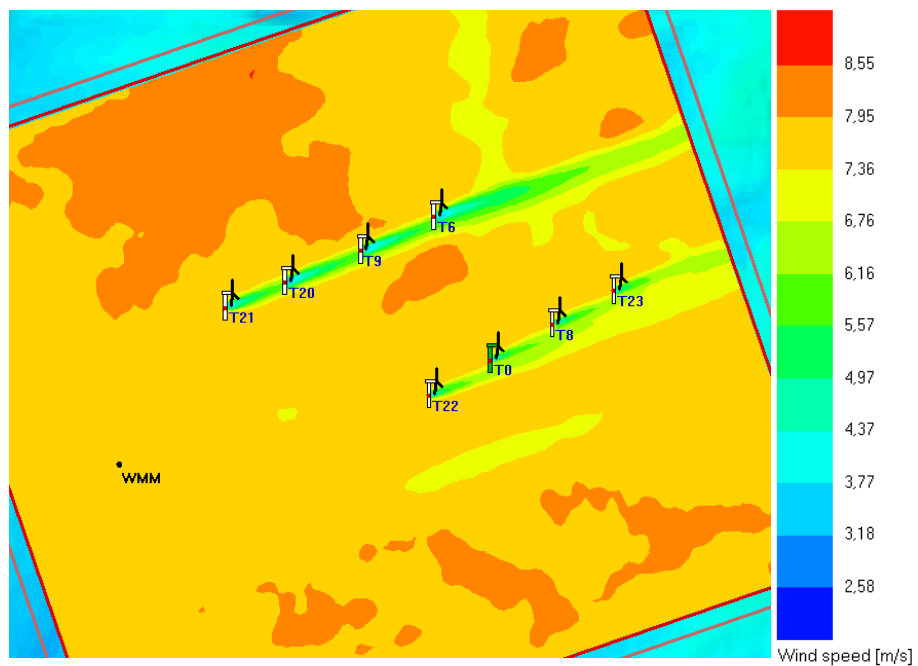


Figure 5.8 - Wind speed contour map obtained with Larsen model in WindStation ( $z=94$  m;  $\theta_{WMM} = 251^\circ$ ;  $V_{WMM,101m} = 7.82$  m/s)

#### 5.4.1. Single wake and multiple wake results

A single wake situation was analyzed by considering the wake region of turbine  $T21$ . For that purpose, the wind speed obtained at turbine  $T20$  was normalized

with respect to the upstream turbine  $T21$ , since this turbine encounters undisturbed flow. The results for the Jensen, Jensen 2D and Larsen models will now be shown.

**Jensen.** Figure 5.9 and Figure 5.10 show the results for turbine  $T20$  when using the Jensen (WindStation) and the Jensen (WindSim) model, plotted together with measurement data. A WDC of 0.075 was used in both models. The following observations can be made:

- Looking at the measurement points, the wind direction interval in which the wake of turbine  $T21$  affects turbine  $T20$  can be roughly estimated as  $\theta \in [235^\circ, 260^\circ]$ . This interval is defined by the green vertical lines of Figure 5.9 and will later be used for error computation.

- Constant velocity deficit: In the Jensen (WindStation) model, the normalized wind speed is constant. It is approximately equal to 0.80 within the region affected by the wake, and equal to 1 outside of it.

- Step in Jensen (WindSim): the curves implicitly defined by the Jensen (WindStation) and Jensen (WindSim) models always matched each other well except for the points that have normalized wind speed values around 0.90. These points, indicated by the red circles in Figure 5.9, form a “step” between the free wind speed region and the wake region. The cause for this is yet unknown.

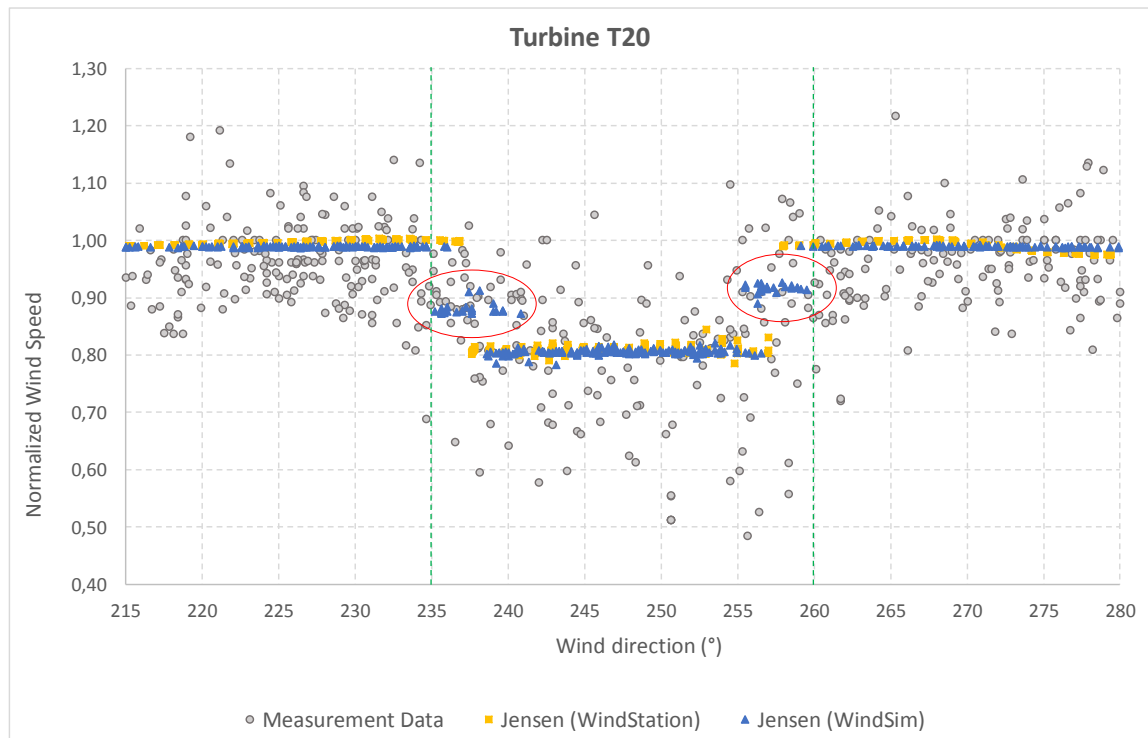


Figure 5.9 – Jensen (WindStation) and Jensen (WindSim) panorama results for turbine T20 and wspd bin of 4-6 m/s.

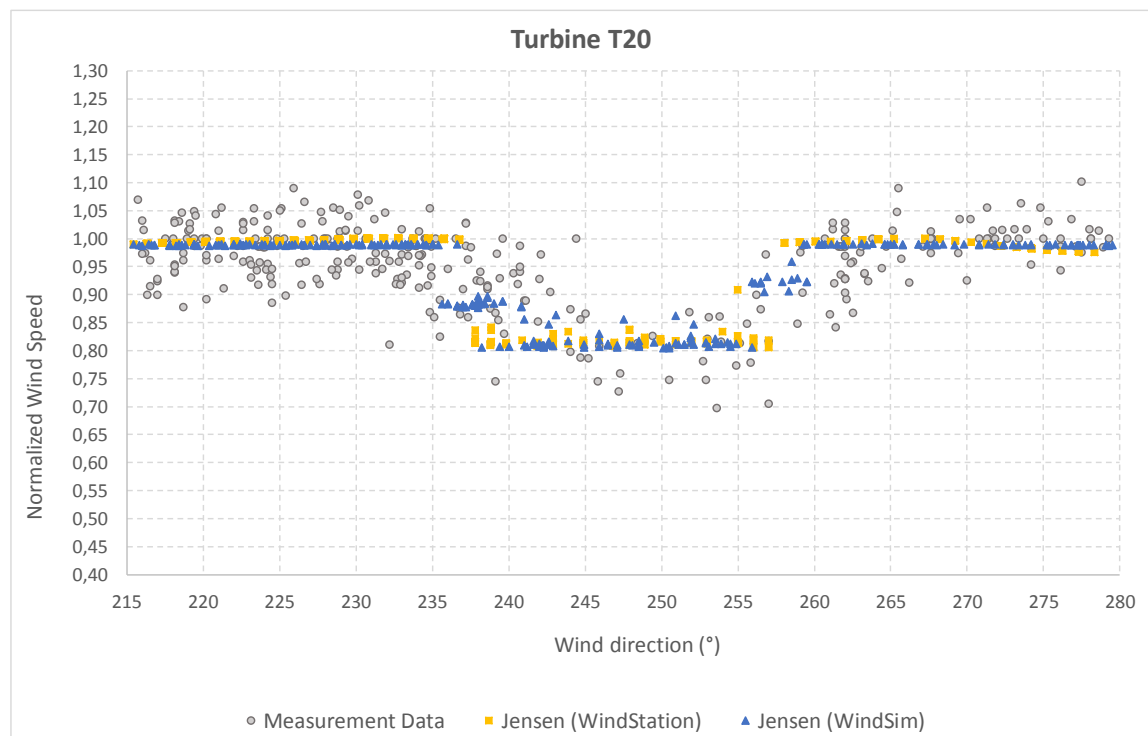
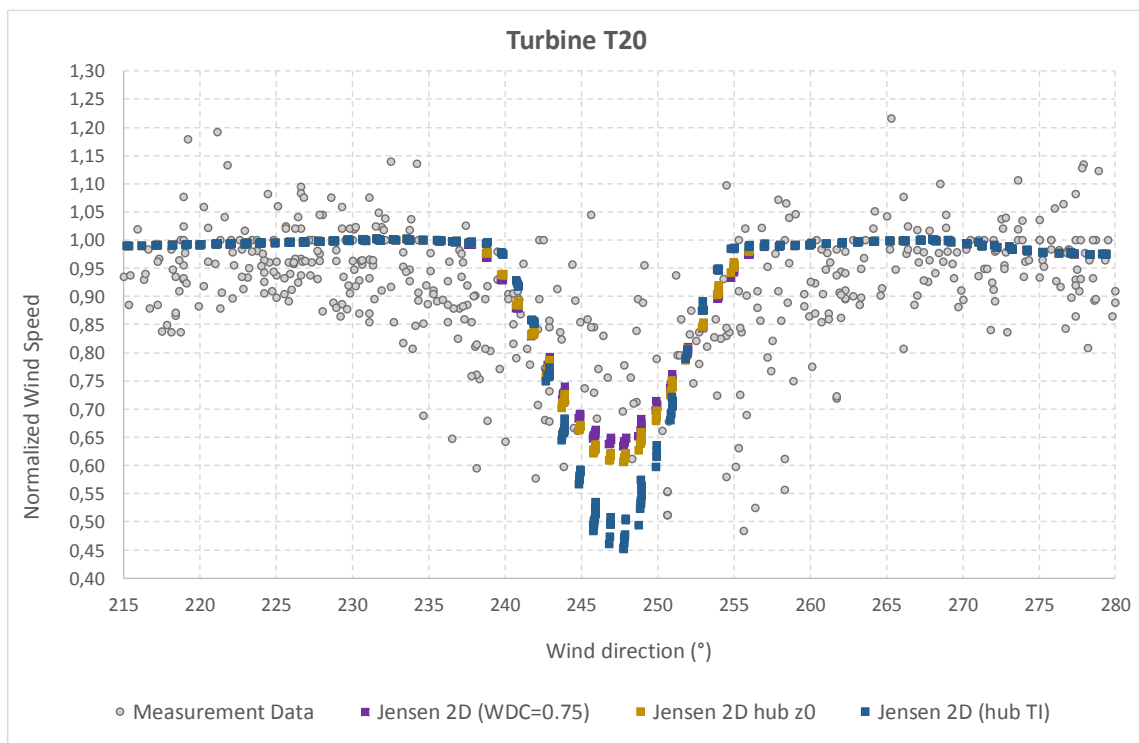


Figure 5.10 - Jensen (WindStation) and Jensen (WindSim) panorama results for turbine T20 and wspd bin of 6-8 m/s.

**Jensen 2D.** Results for turbine *T20* were plotted in Figure 5.11 and Figure 5.12. Three different ways of computing the WDC were tested: a constant WDC of 0.075, the WDC computed with the *hub*  $T_I$  and the WDC computed with the *hub*  $z_0$ . In this case, the wake effects were found to be more pronounced when using the *hub*  $T_I$  WDC, as it can be seen by its curve which was the steepest (deepest valley). On the contrary, the constant 0.075 WDC option seems to be the least affected by the wake effects, as the corresponding curve is the least steep. When comparing with measurement data, all three options seem to overestimate the wake effects. The  $WDC = 0.075$  option was set as the comparison term to the rest of the models.



**Figure 5.11 – Jensen 2D (WindStation) panorama results for turbine T20 and wspd bin of 4-6 m/s.**

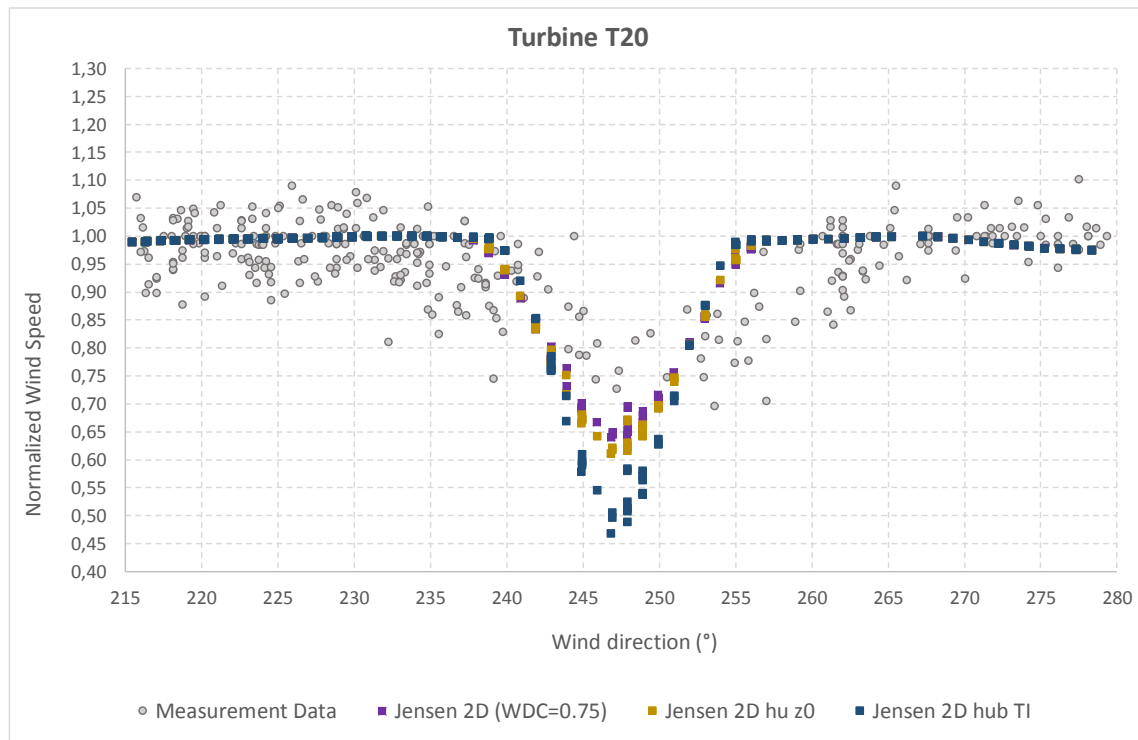


Figure 5.12 - Jensen 2D (WindStation) panorama results for turbine T20 and wspd bin of 6-8 m/s.

**Larsen.** Figure 5.13 and Figure 5.14 show the results obtained with the Larsen (WindStation) and Larsen (WindSim) models, plotted together with the measurement data. The two model curves are notoriously different. The Larsen (WindSim) results showed an excessive wake width and a low velocity deficit. This may lead to the conclusion that the Larsen (WindSim) model underestimated the wake effects. Furthermore, a severe disparity on the results between these two models was found. This may be due to parametrization differences regarding the turbulence intensity. As mentioned in Section 3.1.1.2, the turbulence intensity is computed by Equation 3.8. However, in WindStation results can be corrected *a posteriori* by imposing the turbulence intensity at the meteorological mast, which can be calculated by the Equation 4.1 presented in Section 4.2. In order to evaluate the influence this correction could have on results, three points of Figure 5.14, modelled by Larsen (WindStation), were selected  $[(\theta = 243.9^\circ, V_{normalized} = 0.78); (\theta = 246.9^\circ, V_{normalized} = 0.72); (\theta = 251.9^\circ, V_{normalized} = 0.82)]$  and the turbulence intensity correction was applied. The new computed values of normalized wspd were respectively  $[V_{normalized} = 0.93; V_{normalized} = 0.88; V_{normalized} = 0.86]$  (see Table 5.1). In Figure 5.14, the crosses in blue represent the new points in the chart and the black

arrows represent its transition. The increase in the normalized wspd value led to the conclusion that the turbulence intensity in the mast was higher than the one predicted by Equation 3.8. Whether this correction is applied in WindSim or not, it is yet unknown.

**Table 5.1 -  $T_I$  correction**

$\theta$ [°]	WindStation		
	243.9	246.9	251.9
Modelled $T_I$	11.6%	12.5%	11.2%
Corrected $T_I$ (z=99 m)	22.3%	16.3%	11.8%
Modelled normalized wspd	0.78	0.72	0.82
Normalized wspd with $T_I$ correction	0.93	0.88	0.86

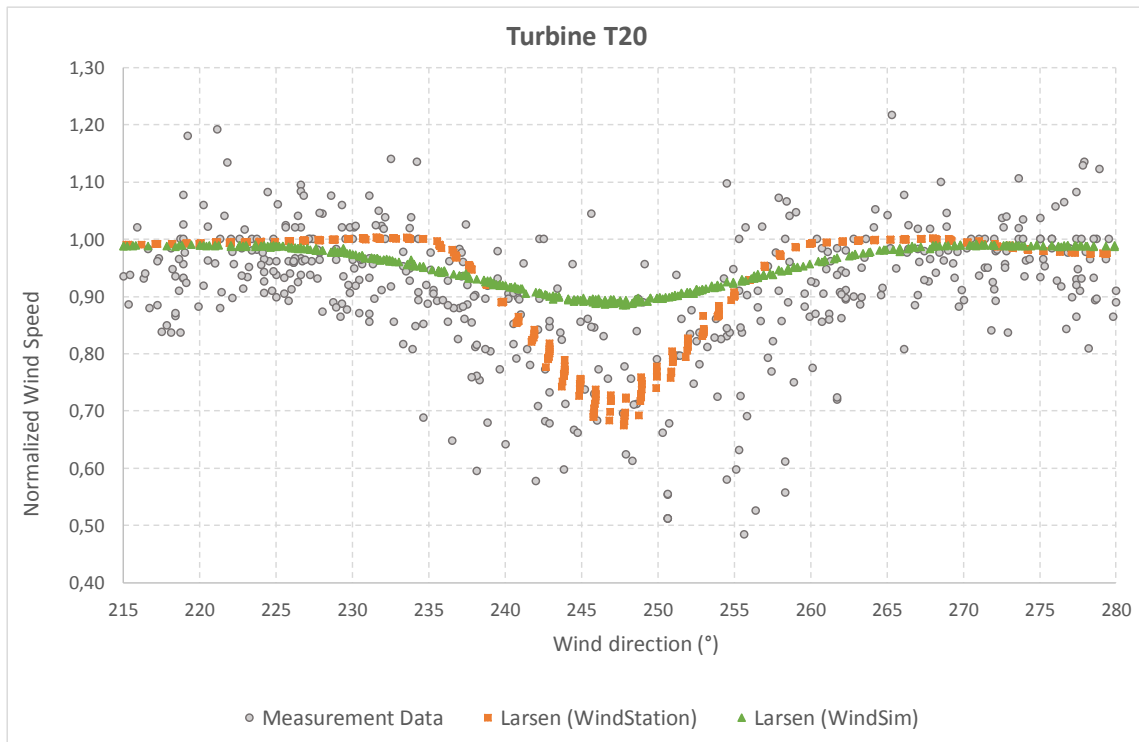


**Figure 5.13 - Larsen (WindStation) and Larsen (WindSim) panorama results for turbine T20 and wspd bin of 4-6 m/s.**

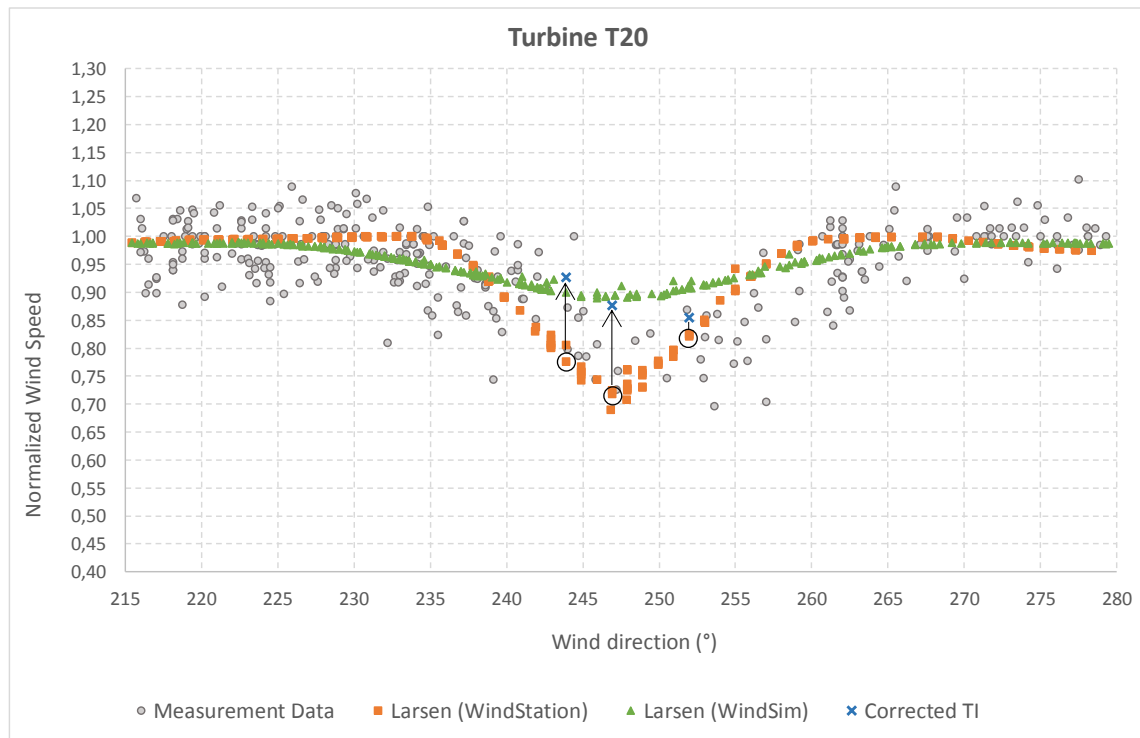


**Figure 5.14 - Larsen (WindStation) and Larsen (WindSim) panorama results for turbine T20 and wspd bin of 6-8 m/s.**

Finally, in Figure 5.15 and Figure 5.16 it was possible to display all the results for turbine *T20*. When comparing the Jensen 2D (WindStation) with the Larsen (WindStation), it is clear that the Larsen curve has a lower steepness and a wider wake width. Note that there were no significant differences in the modelled wake width or velocity deficit when changing from a wind speed bin of 4 – 6 m/s to 6 – 8 m/s. However, when looking only at the measurement data points, the velocity deficit seems to be higher for 4 – 6 m/s than for 6 – 8 m/s.

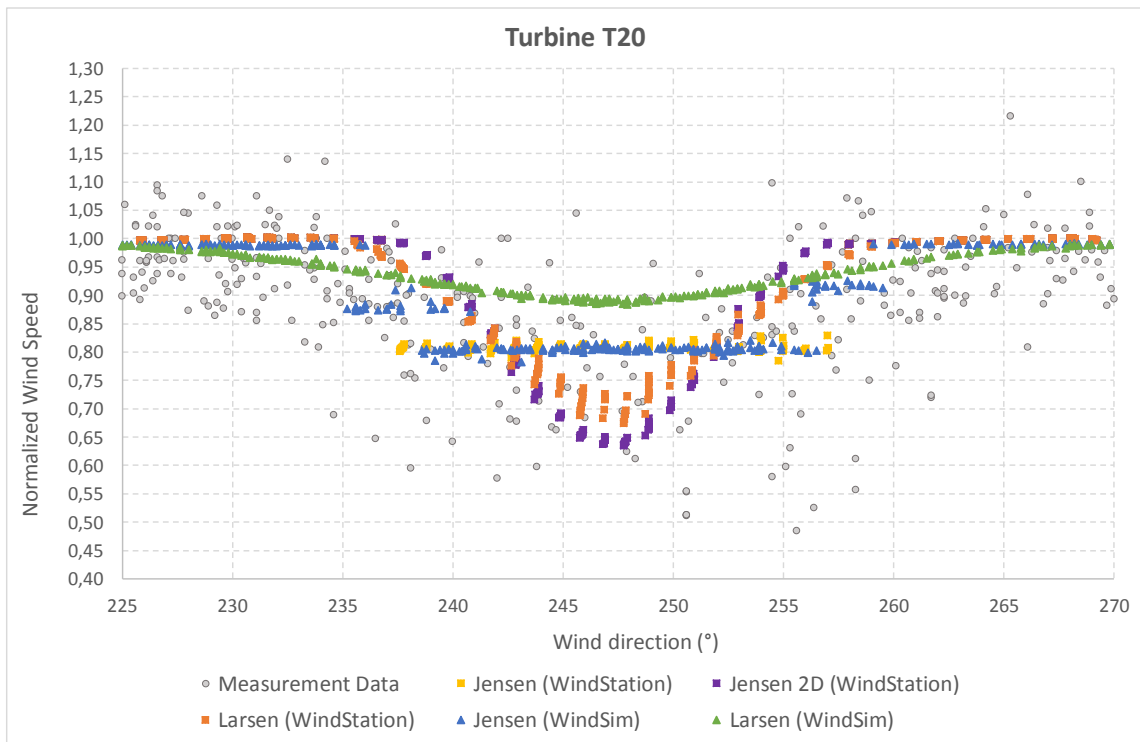


Figure 5.15 – Panorama results obtained in all wake models for turbine T20 and wspd bin of 4-6 m/s.

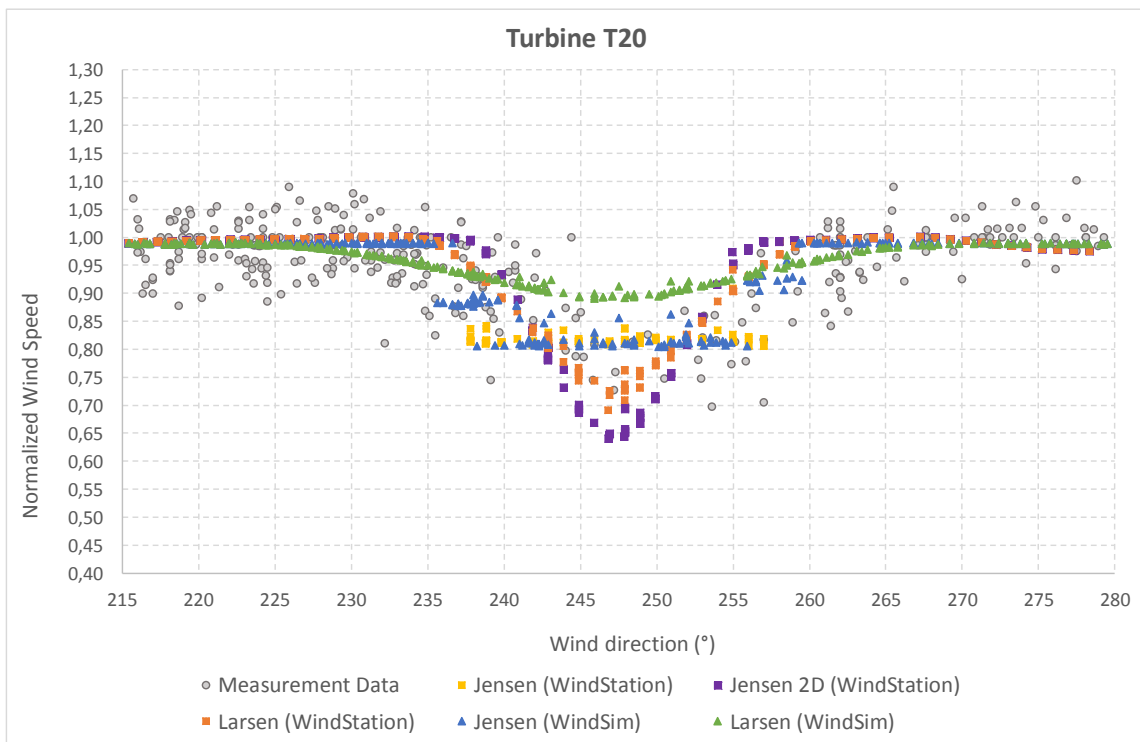


Figure 5.16 - Panorama results obtained in all wake models for turbine T20 and wspd bin of 6-8 m/s.

In order to evaluate how each model has adjusted to the measurement data, a polynomial function that best fits the corresponding model points was first computed. For that purpose, the *Matlab* function *polyfit* was used. Several degrees for the polynomials were tried and the value chosen was 6 for every model except for the Jensen (WindStation). In this last one, a linear function was enough, since its values are approximately constant. Then, the polynomial functions were used as a replacement for the model points, to compute the corresponding error of the adjustment to the measurement data. This error was calculated by summing up all the absolute values of the individual errors for each entry of the measurement data, divided by the number of those entries:

$$\frac{\sum_{i=1}^N |p(\theta_{measured,i}) - V_{normalized_{measured,i}}|}{N} \quad (5.3)$$

where  $p$  is the polynomial corresponding to the model at stake,  $(\theta_{measured,i}, V_{normalized_{measured,i}})$  are the measurement data points and  $N$  is the number of those points.

The range of the abscissa  $\theta_{measured,i}$  of the measurement data points was restricted to the already mentioned wind direction interval  $[235^\circ, 260^\circ]$ . Table 5.2 shows the results obtained:

**Table 5.2 – Error obtained for all five wake models.**

T20	Jensen (WindStation)	Jensen 2D ( $WDC = 0.075$ )	Larsen (WindStation)	Jensen (WindSim)	Larsen (WindSim)
4-6 m/s	0.1012	0.1192	0.1011	0.0947	0.1237
6-8 m/s	0.0794	0.0894	0.0651	0.0652	0.0708

The largest errors were found in Larsen (WindSim) for a 4 – 6 m/s wind speed bin and in Jensen 2D (WindStation) for a 6 – 8 m/s wind speed bin, with values of 0.1237 and 0.0894 respectively. These values strengthened the conclusion that the Larsen (WindSim) underestimated the wake effects and the Jensen 2D ( $WDC = 0.075$ ) overestimated them. On the other hand, lower values were obtained in the Jensen

(WindSim) model than in the Jensen (WindStation) model, which can only be explained by the step points in Jensen (WindSim).

As already shown by Figure 5.6–Figure 5.8, the wind direction sector  $\theta \in [225^\circ; 270^\circ]$  accounts for multiple wake superposition situations. The results obtained for turbines  $T9$  and  $T6$ , which are respectively placed in a double and triple wake region, are presented in Figure 5.17–Figure 5.20. Naturally, if the distance to the lead turbine increases, the wind direction interval in which the wake effect of turbine  $T21$  is noticed, decreases. See for instance the example of Larsen (WindStation) in the 4 – 6 m/s wspd bin: for turbine  $T20$  (Figure 5.15) this interval is approximately  $[236^\circ, 260^\circ]$ , for turbine  $T9$  (Figure 5.17) it is reduced into  $[238^\circ, 257^\circ]$  and for turbine  $T6$  (Figure 5.19) into  $[238^\circ, 256^\circ]$ . However, the effect of the wake superposition in the velocity deficit was hardly noticed, despite the slight increase from turbine  $T20$  to turbine  $T9$ . Overall, the normalized wind speed values obtained in turbines  $T9$  and  $T6$  were similar to the ones in turbine  $T20$ .

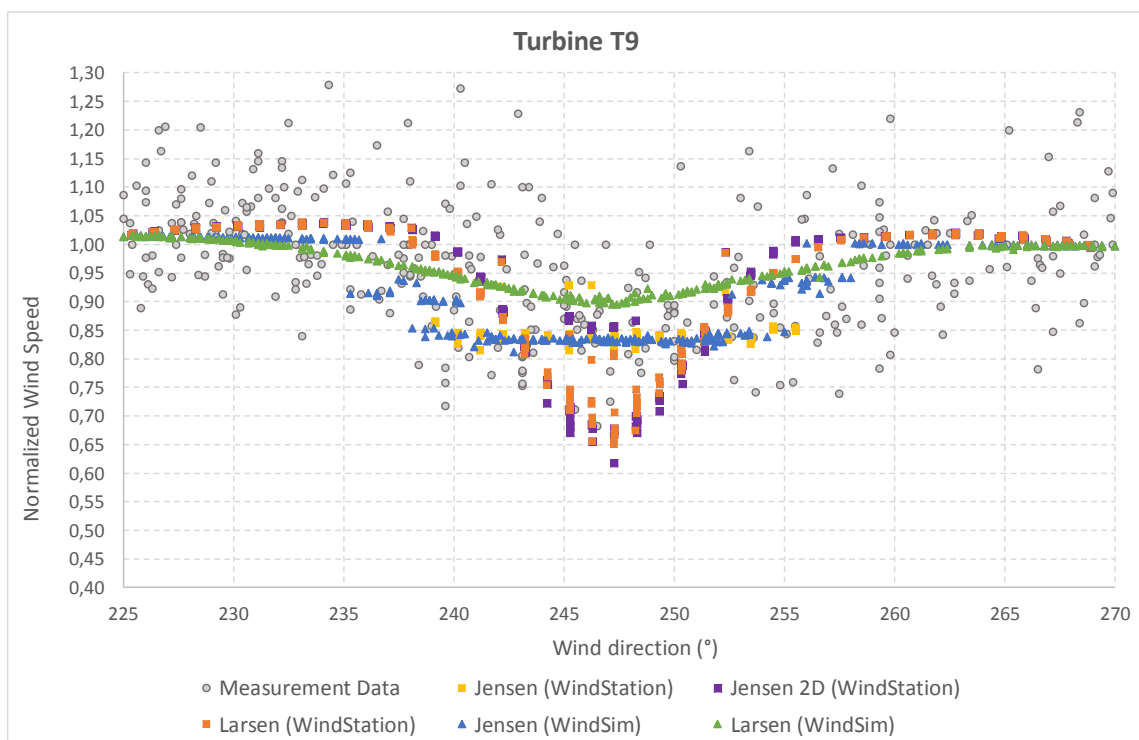


Figure 5.17 - Panorama results obtained in all wake models for turbine  $T9$  and wspd bin of 4-6 m/s.

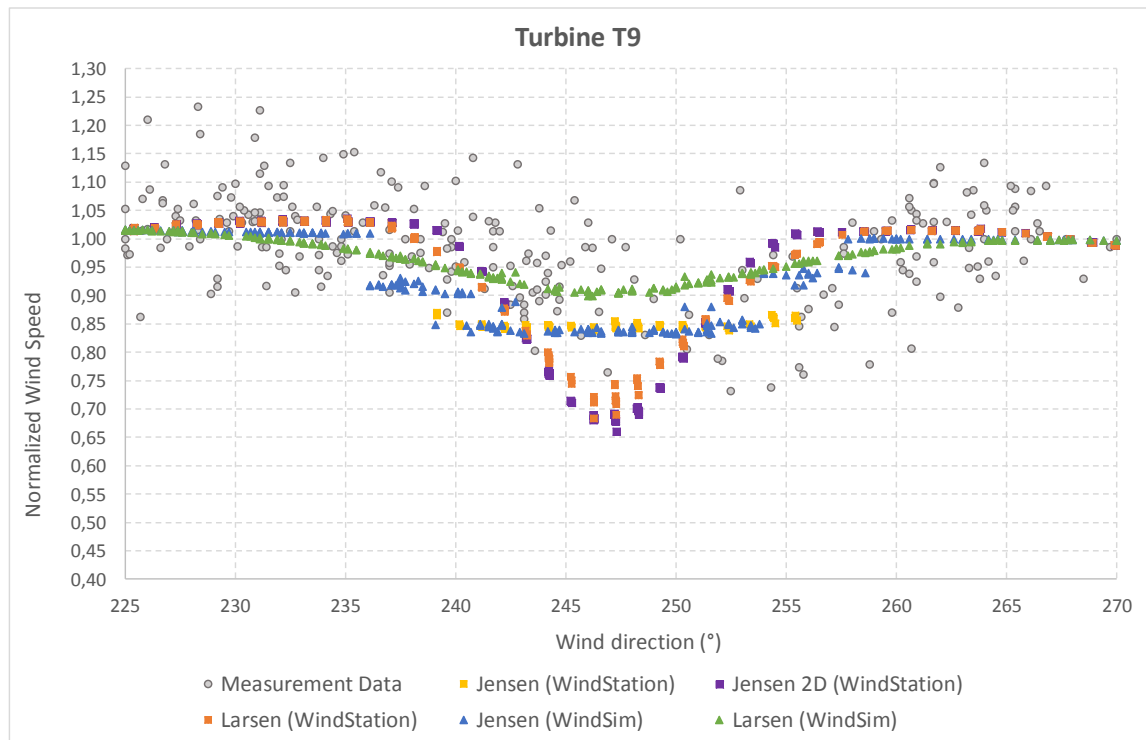


Figure 5.18 - Panorama results obtained in all wake models for turbine T9 and wspd bin of 6-8 m/s.

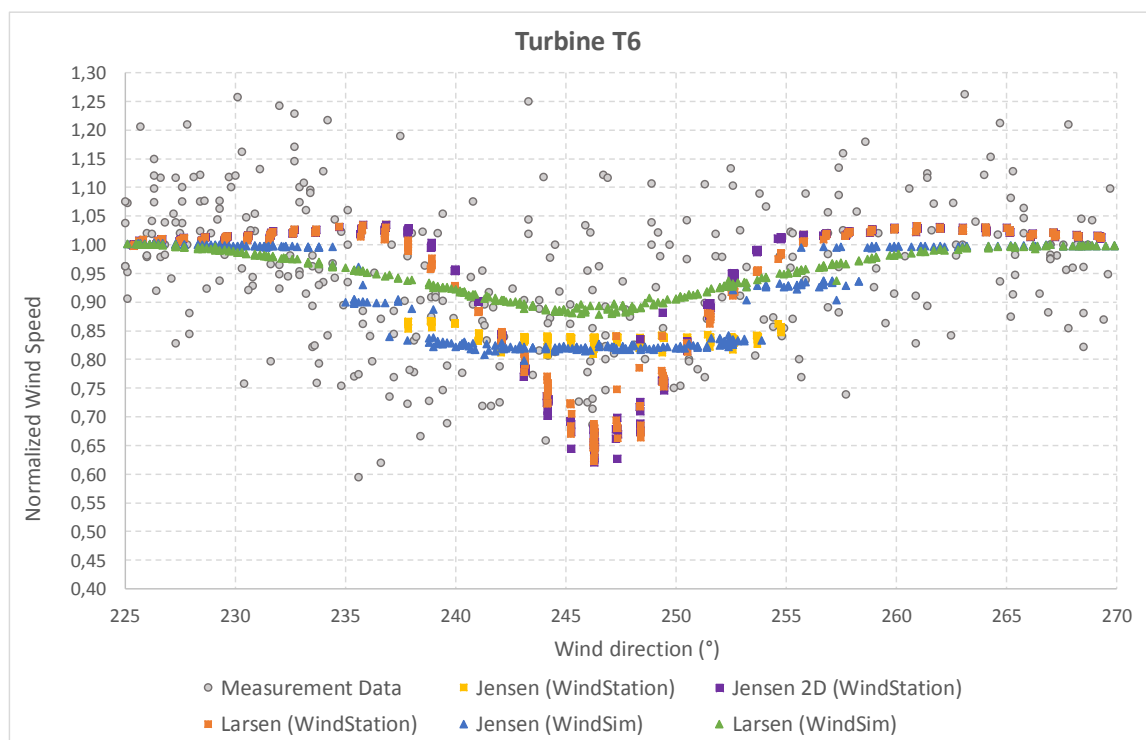


Figure 5.19 - Panorama results obtained in all wake models for turbine T6 and wspd bin of 4-6 m/s.

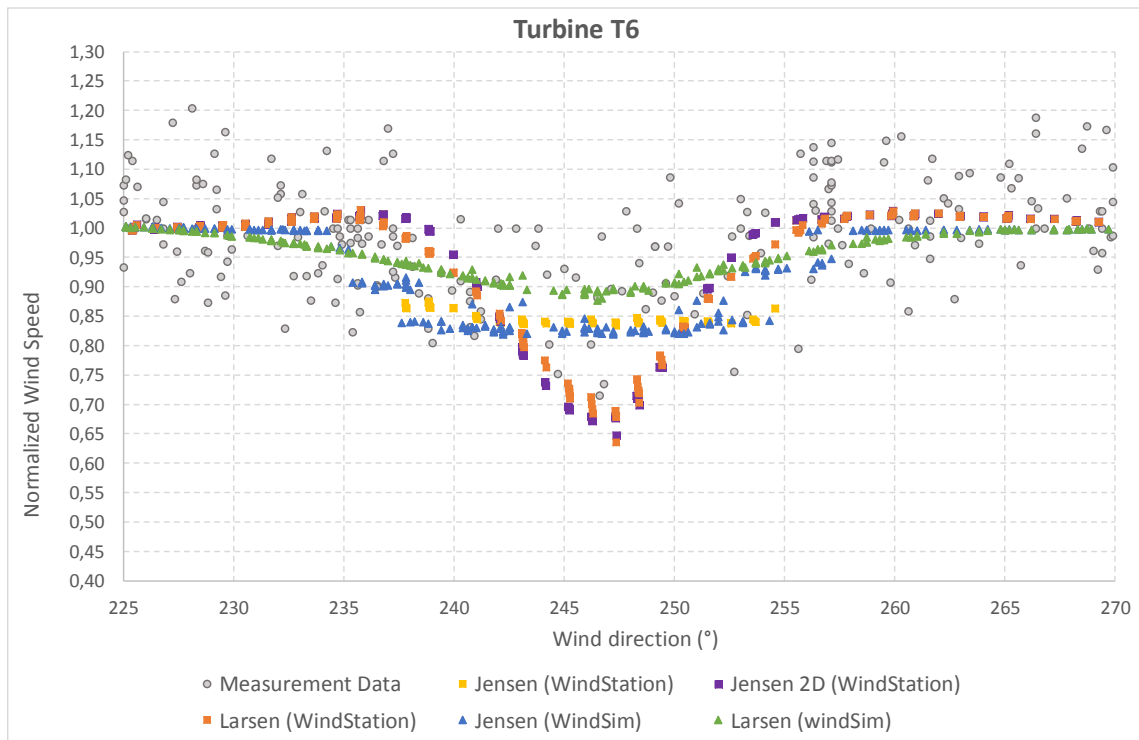


Figure 5.20 - Panorama results obtained in all wake models for turbine T6 and wspd bin of 6-8 m/s.

#### 5.4.2. Offset in wind direction

The same analysis as in the previous section was done to row 2, by normalizing the wind speed with respect to turbine T22. The results obtained are shown in Figure 0.1–Figure 0.6 of APPENDIX B. Although the same conclusions were taken, the offset in wind direction was considerably bigger, due to a larger distance of this row to the meteorological mast. This situation is clearly visible in the results obtained for turbine T0 (wspd bin of 4 – 6 m/s), displayed in Figure 5.21. In fact, the average value of the difference between the measured and the modelled wind direction was calculated and equals  $9.3^\circ$ . The offset was corrected and Figure 5.21 was updated into Figure 5.22. The error was calculated like in the previous section and updated (see Table 5.3); note that it decreased for all models, except for the Larsen (WindSim).

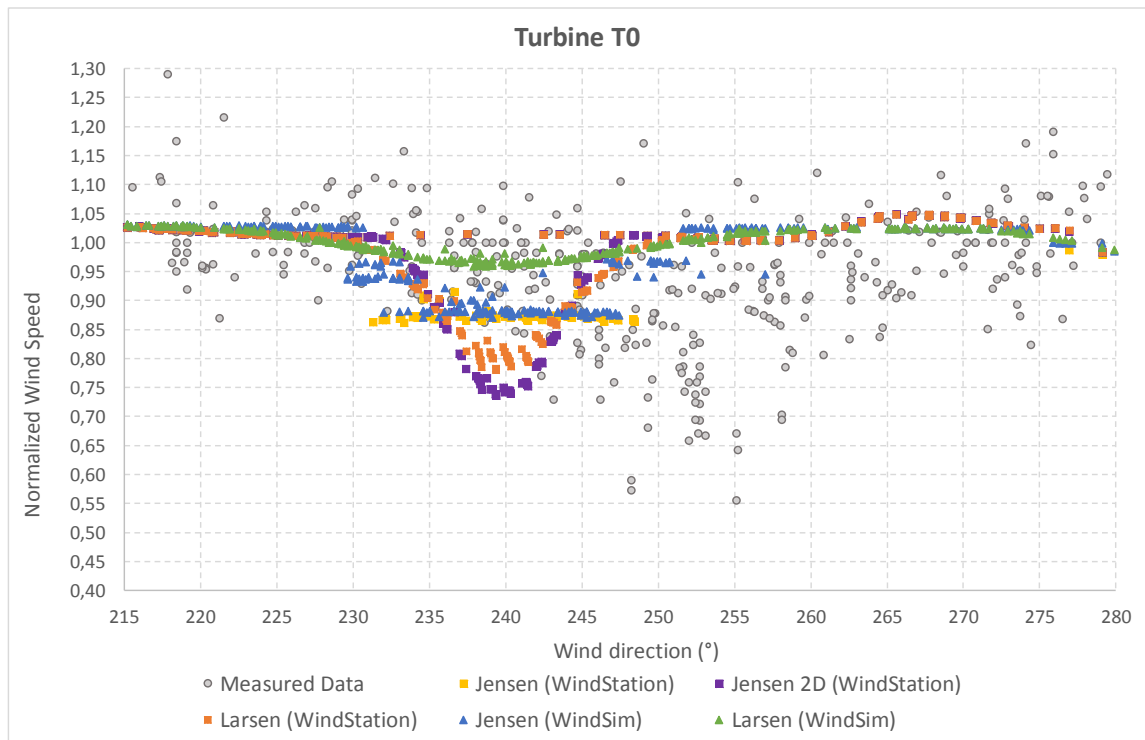


Figure 5.21 - Panorama results obtained in all wake models for turbine T0 and wspd bin of 4-6 m/s.

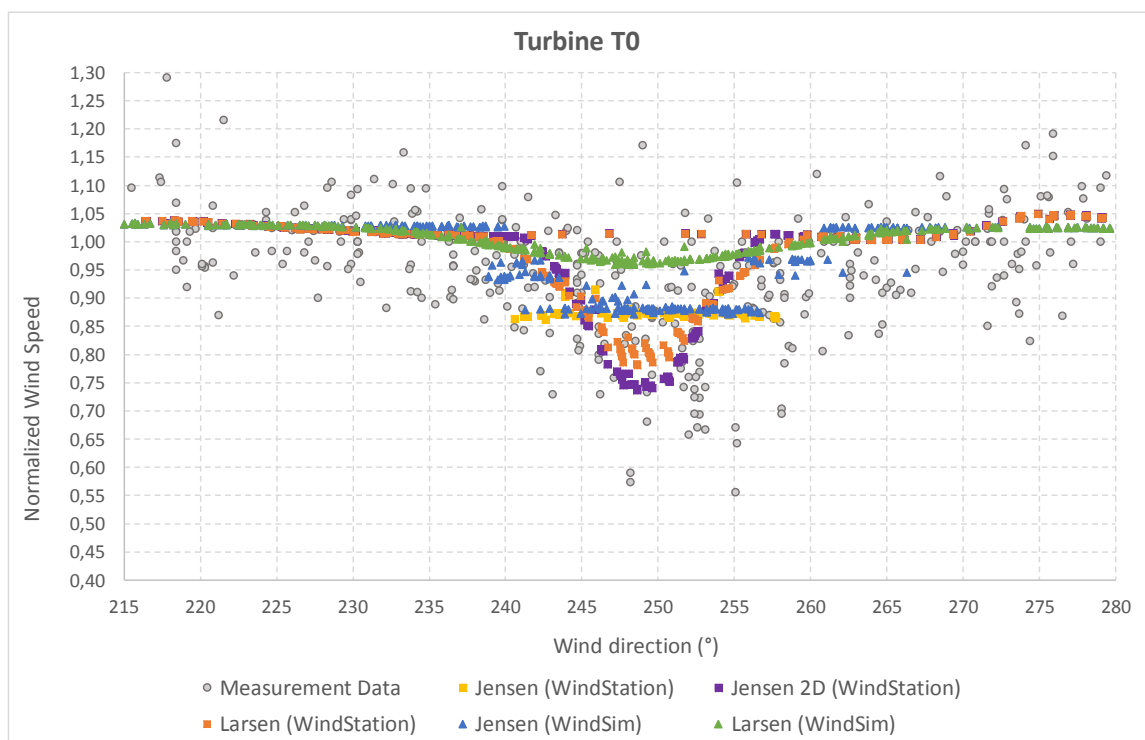


Figure 5.22 – Offset correction: updated panorama results obtained in all wake models for turbine T0 and wspd bin of 4-6 m/s.

**Table 5.3 – Offset correction: updated error obtained for all five wake models**

T0 (4-6 m/s)	Jensen (WindStation)	Jensen 2D (WindStation)	Larsen (WindStation)	Jensen (WindSim)	Larsen (WindSim)
Normal	0.0935	0.1323	0.1125	0.0925	0.0776
With offset correction	0.0928	0.0989	0.0906	0.0917	0.0883

### 5.4.3. Effective power of a wind turbine

As wind flows across a wind turbine, the power available ( $P$ ) in the wind is given by (Tong et al., 2012):

$$P = \frac{1}{2} \rho_{air} A V_{\infty}^3$$

where  $\rho_{air}$  is the air density,  $A$  is the rotor swept area and  $V_{\infty}$  is the incoming wind speed at hub height. Naturally, not all this power is generated by the wind turbine. In WindStation, the effective wind turbine power is computed by interpolating the effective velocity deficit given by Equation 3.25 (see Section 3.1.3) into the measured power curve of the respective wind turbine.

It should be interesting to compare results obtained for wind speed deficits with wind turbine effective power. Figure 5.23 plots the power obtained in row 1 wind turbines for the same case showed earlier in Figure 5.6–Figure 5.8, together with measurement data. The values for effective power were normalized with the wind turbine rated power and are displayed in percentage.

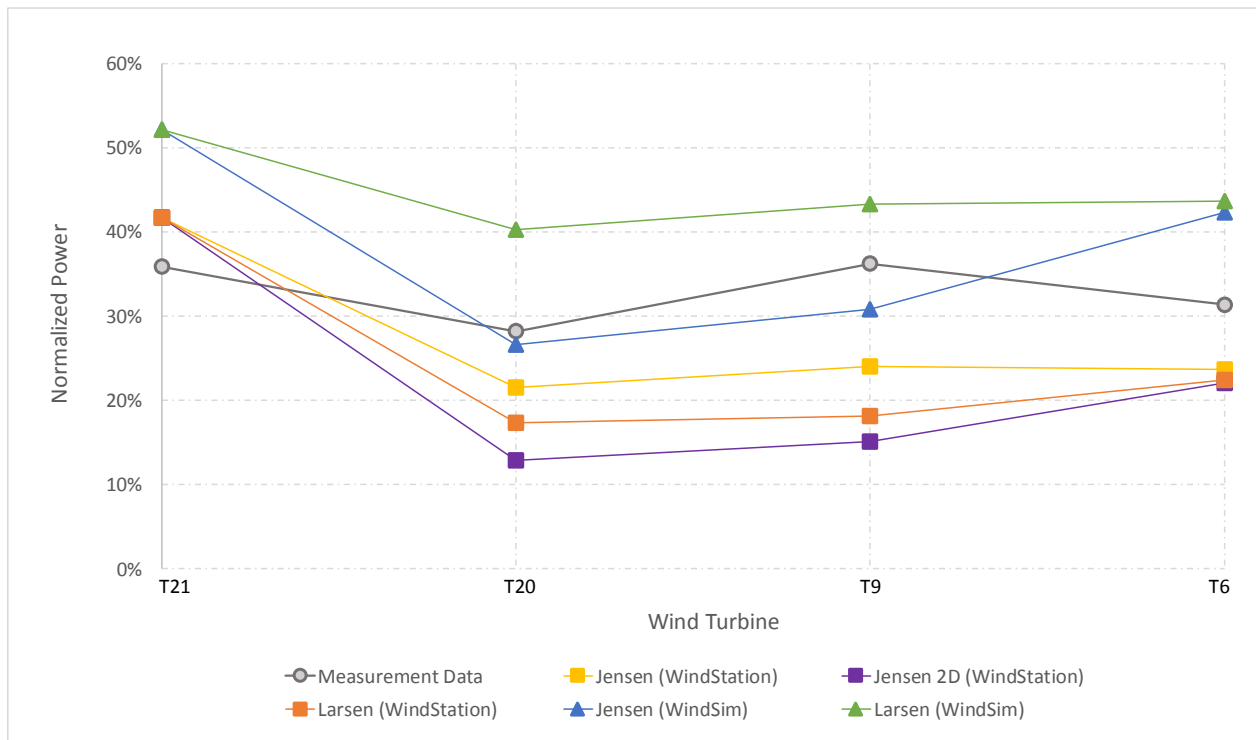


**Figure 5.23 – Normalized effective wind power computed in all wake models**  
 $(\theta_{WMM} = 251^\circ; V_{WMM,101m} = 7.82 \text{ m/s})$ .

Note that for all wake models, there was a significant power drop between turbine  $T21$  and turbine  $T20$ . Then, it slightly increased until turbine  $T6$ . However, the measurement data showed an unpredictable power behavior. It is interesting to see that the Jensen 2D wake model severely overestimated the power loss, which is coherent with the overestimation of velocity deficit estimated in the previous sections. The opposite conclusion can be also taken from the Larsen (WindSim) wake model. Furthermore, a considerable difference between the Jensen (WindStation) and the Jensen (WindSim) wake model was detected, which goes against the similarity shown in the  $wspd$  deficit results. In order to have more detailed conclusions, this analysis should be performed to a large number of cases.



## 6. CONCLUDING REMARKS

The performance of the WindStation wake models has been evaluated using measurement data and the software package WindSim. A panorama simulation was carried out by inputting the meteorological mast data and analyzing the wind direction sectors availability. The velocity deficit results were compared with measurement data of the wind turbines (at hub height), and with results from a similar simulation run in WindSim.

One of the main setbacks of this work was dealing with uncertainties in the measurement data, more specifically regarding the offset in wind direction between the meteorological mast and the wind turbines. This is why the velocity deficit was always normalized against the upstream wind turbine. Another setback was the lack of measurement data. A larger set of measurement data would strengthen the evaluation of these models by providing the chance to analyze the wake effects in more wind direction sectors and different turbine spacing.

Distinct behavior was found when comparing results from WindStation and WindSim. The Jensen wake model had a similar performance in both software packages, except for points close to the boundary between the wake and the free stream flow. The Larsen wake model results were significantly different from one software to another, most likely due to differences in the turbulence intensity computation.

When comparing the modelled results with the measurement data, the Jensen 2D wake model was found to overestimate the velocity deficit. On the contrary, the Larsen (WindSim) showed a far too wide wake and an underestimation of the velocity deficit. The error of the modelled results compared to the measurement data, that was computed in Section 5.4.1, supported these conclusions.

The validation of the wake models is still incomplete and further investigation is recommended to assess the influence of the turbulence intensity correction in the Jensen 2D and Larsen wake models. Moreover, it should be interesting to reproduce the analysis done on the effective power of a single wind turbine (reported in Section 5.4.3) in a larger set of time records, and then to compute the total output power of the wind farm.



---

## REFERENCES

- Abramovich, G.N. 1963. *The Theory of Turbulent Jets*. Cambridge, Mass.: Press, MIT.
- Ainslie, J.F. 1985. "Development of an Eddy Viscosity Model for Wind Turbine Wakes." In *Proc. 7th BWEA Wind Energy Conf*, Oxford, 61–66.
- Barthelmie, R.J. et al. 2011. *Flow and Wakes in Large Wind Farms : Final Report for UpWind WP8 Risø-R-Report*.
- Bossanyi, E.A. et al. 1980. "The Efficiency of Wind Turbine Clusters." In *Proc. 3rd Int. Symp. on Wind Energy Systems*, Lyngby, 401–16.
- Crespo, A., and J. Hernández. 1989. "Numerical Modelling of the Flow Field in a Wind Turbine Wake." In *Proc. 3rd Joint ASCE/ASME Mechanics Conf.*, La Jolla, CA, 121–27.
- Crespo, A., J. Hernández, and S. Frandsen. 1999. "Survey of Modelling Methods for Wind Turbine Wakes and Wind Farms." *Wind Energy* 2: 1–24.
- Van Doormaal, J.P., and G.D. Raithby. 1984. "Enhancements of the Simple Method for Predicting Incompressible Fluid Flows." *Numerical Heat Transfer* 7: 147–63.
- Emeis, S., and S. Frandsen. 1993. "Reduction of Horizontal Wind Speed in a Boundary Layer with Obstacles." *Boundary-Layer Meteorol.* 64: 297–305.
- Frandsen, S. 2007. "Turbulence and Turbulence-Generated Structural Loading in Wind Turbine Clusters." Technical University of Denmark.
- "Global Mapper 19.1." <http://www.bluemarblegeo.com/products/global-mapper.php>.
- GWEC. 2018. "Global Cumulative Installed Capacity 2001-2017." <http://gwec.net/global-figures/graphs/> (August 20, 2007).
- Hayase, T., J.A.C. Humphrey, and R. Greif. 1992. "A Consistently Formulated Quick Scheme for Last and Stable Convergence Using Finite-Volume Iterative Calculation Procedures." *Journal of Computational Physics* 98: 108–18.
- Ishihara, T., A. Yamaguchi, and Y. Fujino. 2004. *Global Wind Development of a New Wake Model Based on a Wind Tunnel Experiment*.
- Janssen, J.A.J. 2012. "Development of a Wind Farm Power Forecast Model." MeteoConsult, Delft University of technology, Eindhoven University of Technology.

- Jensen, N.O. 1983. "A Note on Wind Generator Interaction." (Risø-M;No. 2411).
- Larsen, G.C. 1988. "A Simple Wake Calculation Procedure." (Risø-M;No. 2760).
- Lissaman, P.B.S. 1979. "Energy Effectiveness of Arbitrary Arrays of Wind Turbines." *J. Energy* 3: 323–28.
- Lopes, A.G. 2018. "WindStation User's Manual."
- Meissner, C. 2015. "WindSim Getting Started."
- Otto, N., and R. Raguzzi. 1987. "A Simple Model for Cluster Efficiency." In *EWEC'86. Proceedings*, eds. W. Palz and E. Sesto. Rome, 407–10.
- Patankar, S.V. 1980. *Numerical Heat Transfer and Fluid Flow*. Washington, D.C.: Hemisphere Publishing Corporation.
- Réthoré, P-E.M. 2009. *Wind Turbine Wake in Atmospheric Turbulence*. Roskilde: Risø National Laboratory for Sustainable Energy (Risø-PhD; No. 53(EN)).
- Réthoré, P-E.M. et al. 2009. "Systematic Wind Farm Measurement Data Filtering Tool for Wake Model Calibration." In *European Offshore Wind Conference(EOW2009)*, Stockholm.
- Taylor, P.A. 1980. "On Wake Decay and Row Spacing for WECS Farms." In *Proc. 3rd Int. Symp. on Wind Energy Systems*, Lyngby, 451–68.
- Tian, L. et al. 2015. "Development and Validation of a New Two-Dimensional Wake Model for Wind Turbine Wakes." *Journal of Wind Engineering and Industrial Aerodynamics* 137: 90–99.
- Tong, W., S. Chowdhury, J. Zhang, and A. Messac. 2012. "Impact of Different Wake Models On the Estimation of Wind Farm Power Generation." *12th AIAA Aviation Technology, Integration, and Operations (ATIO) Conference and 14th AIAA/ISSM* (September): 1–13.

## APPENDIX A

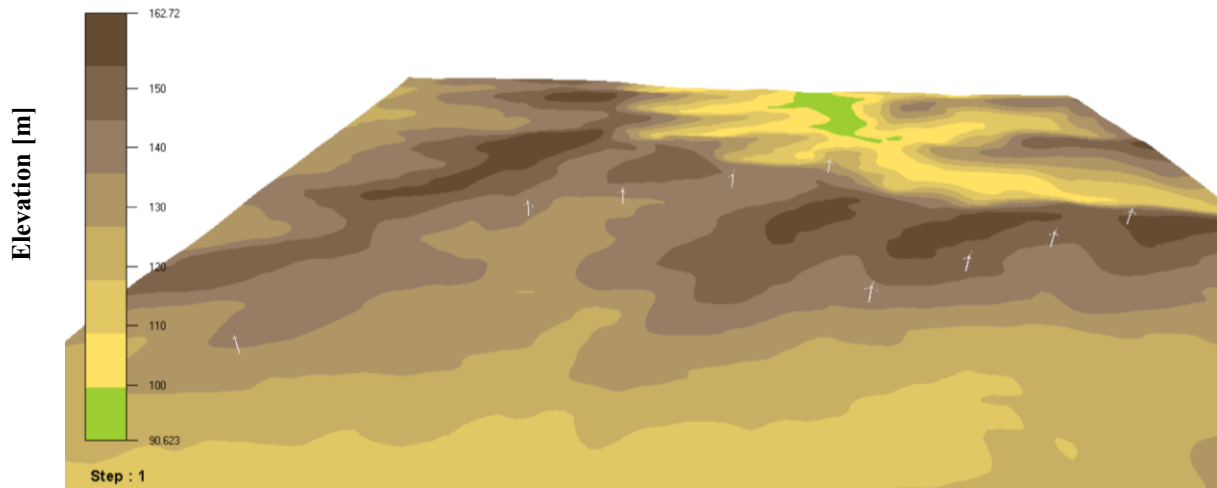


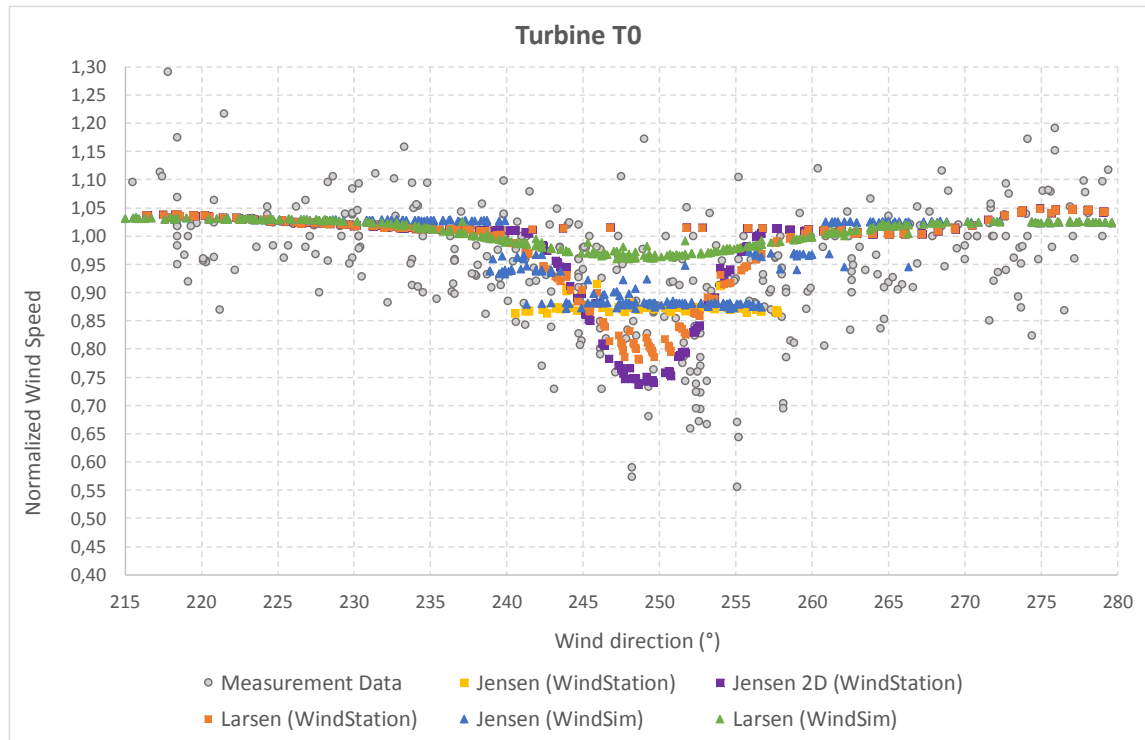
Figure 0.1 – WindSim 3D layout of the wind farm

Table 0.1 – Wind turbines details: row number, turbine name, turbine type and altitude (z) in meters

Row	Turbine name	Turbine type	z (m)
Row 1	T0	Vestas V90	144,4
	T8	Vestas V90	144,6
	T22	Vestas V90	135,6
	T23	Vestas V90	151,5
Row 2	T6	Vestas V112	140
	T9	Vestas V112	141,1
	T20	Vestas V112	133,1
	T21	Vestas V112	137,2



## APPENDIX B



**Figure 0.1 - Panorama results obtained in all wake models for turbine T0 and wspd bin of 4-6 m/s.**

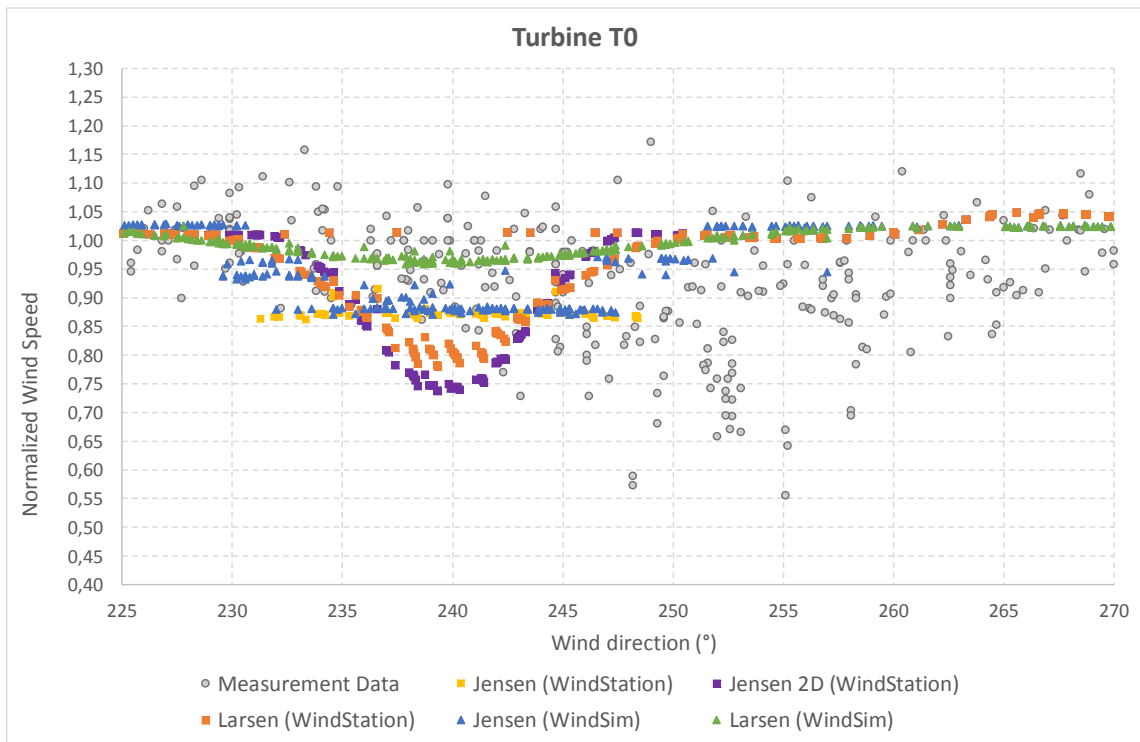


Figure 0.2 - Panorama results obtained in all wake models for turbine T0 and wspd bin of 6-8 m/s.

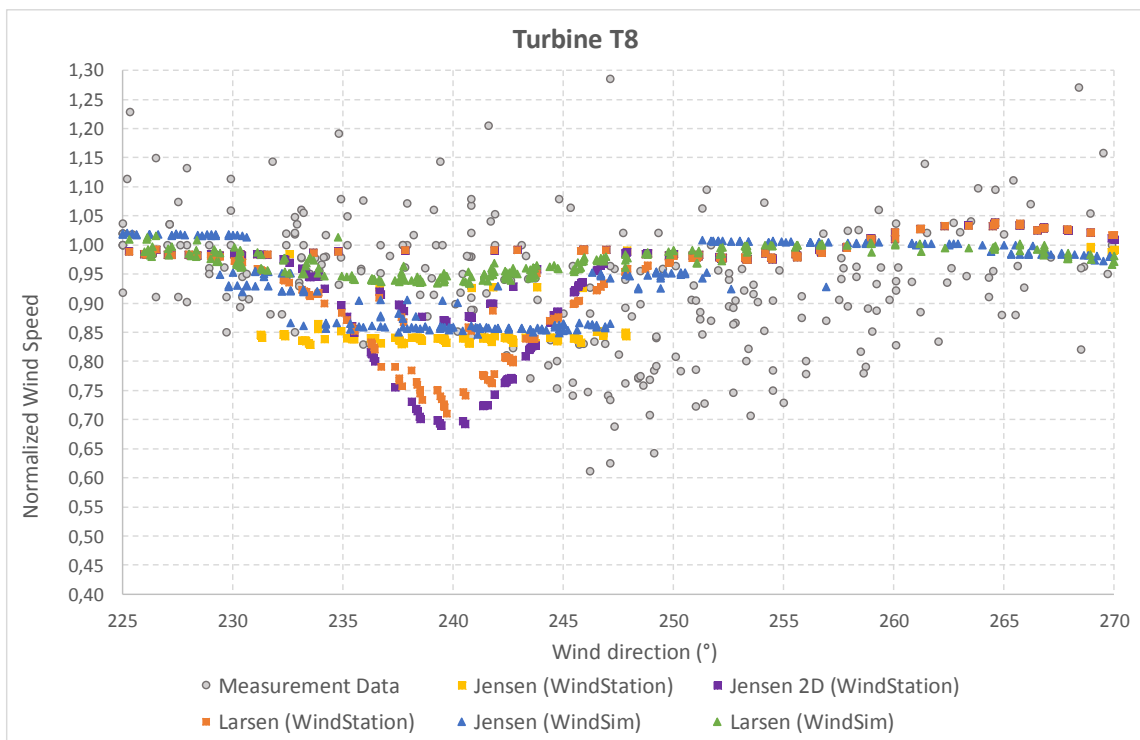
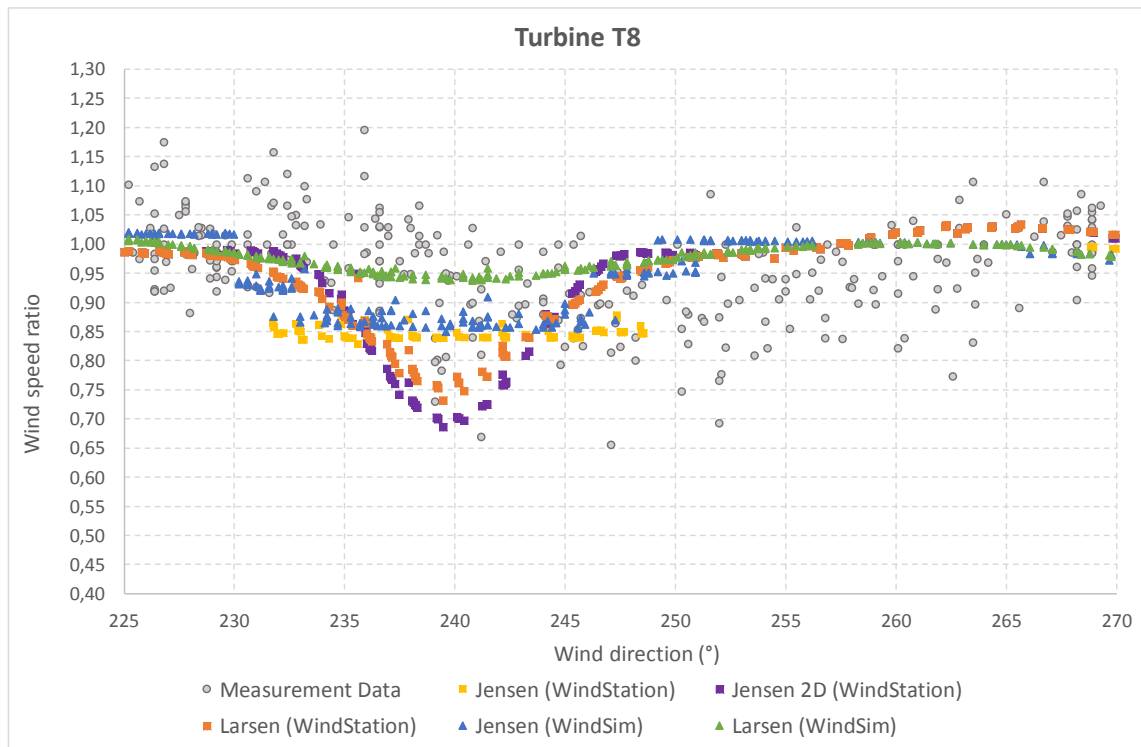
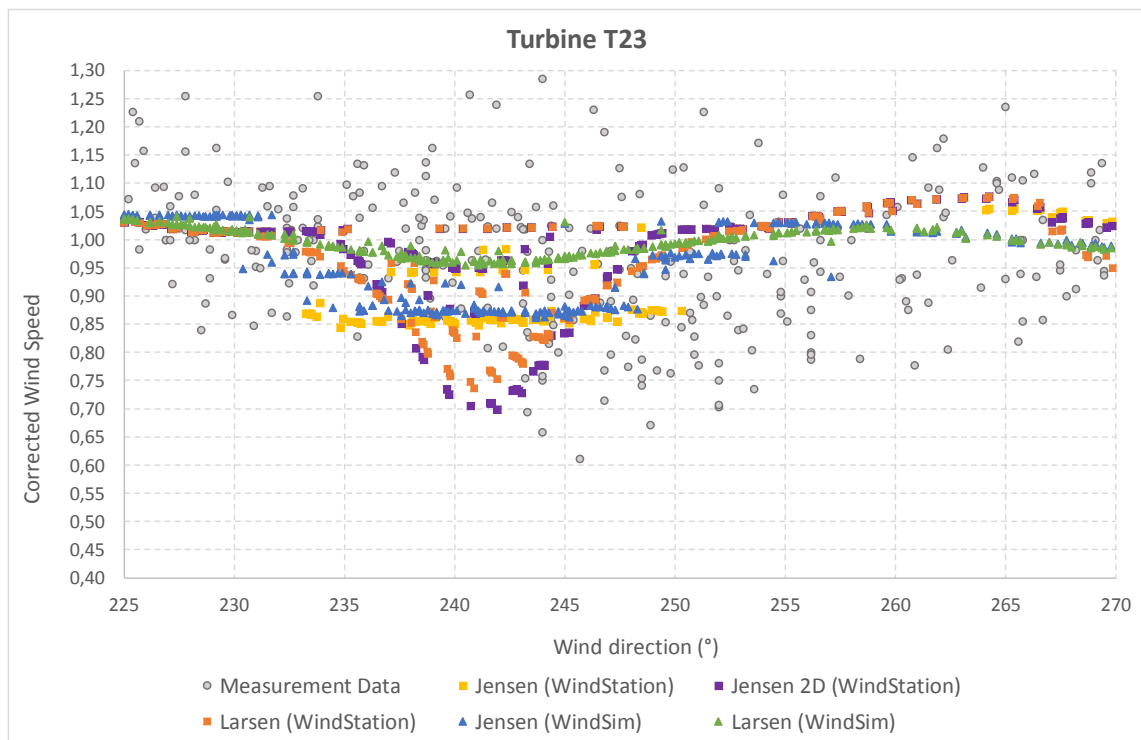


Figure 0.3 - Panorama results obtained in all wake models for turbine T8 and wspd bin of 4-6 m/s.



**Figure 0.4 - Panorama results obtained in all wake models for turbine T8 and wspd bin of 6-8 m/s.**



**Figure 0.5 - Panorama results obtained in all wake models for turbine T23 and wspd bin of 4-6 m/s.**

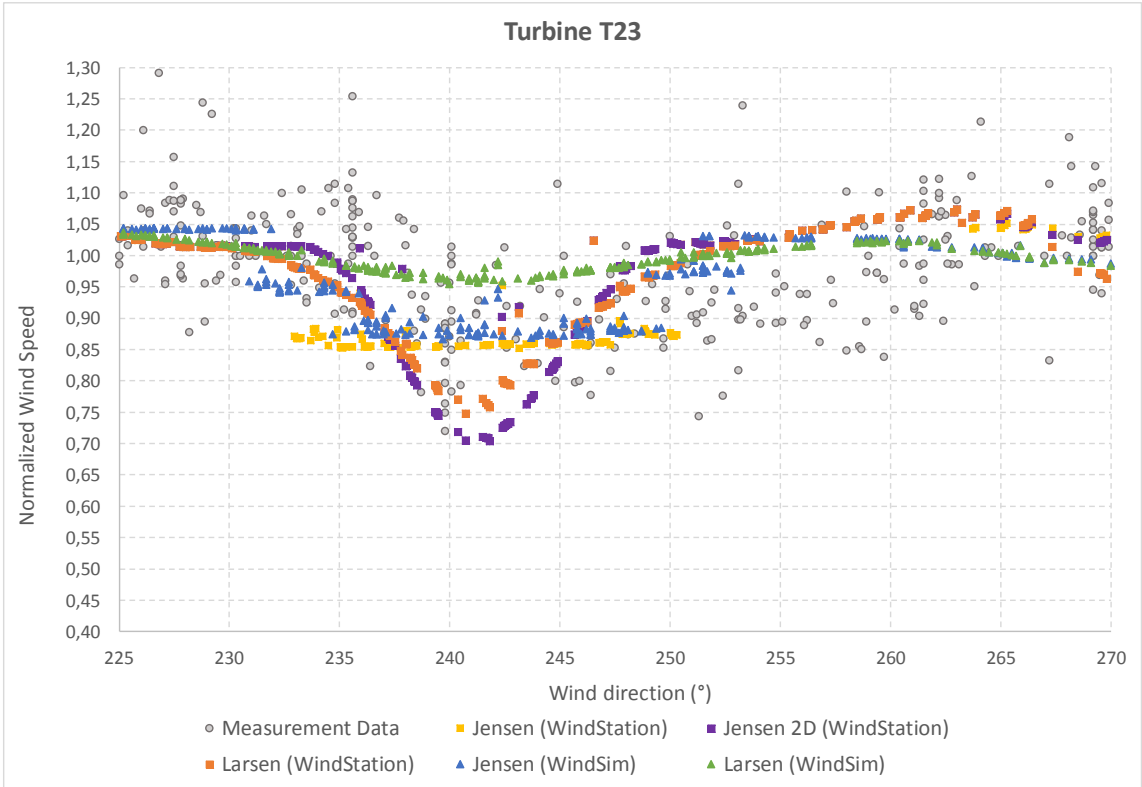


Figure 0.6 - Panorama results obtained in all wake models for turbine T23 and wspd bin of 6-8 m/s.

Fehler! Verweisquelle konnte nicht gefunden werden.

---